

37p

NASA TECHNICAL MEMORANDUM



(NASA TM X-957)

NASA TM X-957

X64 13388*
Page 2

(NASA TM X-957) INVESTIGATION OF STABILITY
CHARACTERISTICS OF STABILITY OF THE HOYLE AND
MERCHISEY ENTRY CAPSULES AT MACH NUMBERS 3
AND 2.5 R.L. Kruse, et al (NASA) Apr.
1964 35 p

Unclas
90/99 24441

COMP
MEAS
GEMI
AT M

by Rob
and B
Ames
Moffet

NATIONAL A

Sp-

37
reg

CASE FILE COPY

~~CONFIDENTIAL~~

COMPARISON OF FREE-FLIGHT MEASUREMENTS OF STABILITY
OF THE GEMINI AND MERCURY ENTRY CAPSULES
AT MACH NUMBERS 3 AND 9.5

By Robert L. Kruse, Gerald N. Malcolm, and
Barbara J. Short

Ames Research Center
Moffett Field, Calif.

~~CONFIDENTIAL~~
Downgraded at 5 year intervals;
~~CONFIDENTIAL~~

CLASSIFIED DOCUMENT - TITLE UNCLASSIFIED
This material contains information affecting the
national defense of the United States within the
meaning of the espionage laws, Title 18, U.S.C.,
Secs. 793 and 794, the transmission or revelation
of which in any manner to an unauthorized person
is prohibited by law.

NATIONAL AERONAUTICS AND SPACE ADMINISTRATION

~~CONFIDENTIAL~~

~~CONFIDENTIAL~~

COMPARISON OF FREE-FLIGHT MEASUREMENTS OF STABILITY
OF THE GEMINI AND MERCURY ENTRY CAPSULES
AT MACH NUMBERS 3 AND 9.5*

By Robert L. Kruse, Gerald N. Malcolm, and
Barbara J. Short

Ames Research Center
Moffett Field, Calif.

SUMMARY

13388

The stability and drag of models of the Gemini entry capsule were measured in free flight at Mach numbers near 3 and 9.5 for comparison with results from similar tests of models of the Mercury entry capsule. It was found that with the center of gravity located at the center of volume both configurations were statically stable and dynamically unstable in the angle-of-attack range tested (from 2° to 16°). The small changes in shape from the Mercury to the Gemini capsule increased the drag about 2 percent and increased the initial ($\alpha = 0$) static stability at both Mach numbers. At $M = 3$ the dynamic instability of the Gemini configuration decreases with increasing amplitude of oscillation; whereas at $M = 9.5$ the dynamic instability is nearly constant at amplitudes of oscillation greater than about 6° .

conf.

A 57402

INTRODUCTION

Project Gemini is planned as the next step to succeed the now completed Mercury project in the manned space flight program. The two-man Gemini entry capsule is basically an enlarged Mercury capsule with small changes in blunt-face curvature and afterbody geometry. In support of Project Gemini, a limited experimental investigation was conducted to determine whether these differences would have an appreciable effect on the aerodynamic characteristics. Experimental measurements of the aerodynamic characteristics of the Mercury configuration are summarized in references 1 and 2.

In the present investigation, the stability and drag of models of the Gemini entry capsule were measured in the Ames Pressurized Ballistic Range and the Ames Supersonic Free-Flight Wind Tunnel at Mach numbers near 3 and 9.5 and at nominally full-scale Reynolds numbers for comparison with the results from similar tests reported in reference 3.

SYMBOLS

A frontal area, sq ft

C_D drag coefficient, $\frac{\text{drag}}{q_\infty A}$, dimensionless

*Title, Unclassified

~~CONFIDENTIAL~~

$C_{L\alpha}$	lift-curve slope, per radian
C_m	pitching-moment coefficient, $\frac{\text{pitching moment}}{q_\infty A d}$, dimensionless
$C_{m\alpha_i}$	$\frac{\partial C_m}{\partial \alpha}$ at $\alpha = 0^\circ$ pitching-moment-curve slope at $\alpha = 0^\circ$, per radian
$(C_{mq} + C_{m\dot{\alpha}})$	damping-in-pitch derivative, $\frac{\partial C_m}{\partial q(d/V)} + \frac{\partial C_m}{\partial \dot{\alpha}(d/V)}$, dimensionless
$C_{N\alpha}$	normal-force-curve slope, per radian
d	maximum diameter, ft
I	moment of inertia about a transverse axis through the center of gravity, $\text{m}\sigma^2$, slug-ft ²
$K_{1,2,3}$	constants in equation (1), deg
m	mass of model, slugs
M	Mach number
p	roll parameter, $\frac{\text{roll rate}}{\text{velocity}}$, radians/ft
q	angular pitching velocity, radians/sec
q_∞	free-stream dynamic pressure, lb/sq ft
R	Reynolds number based on maximum diameter and free-stream conditions, dimensionless
V	velocity along flight path, ft/sec
x	distance along flight path, ft
x_{cg}	axial distance from model nose to center-of-gravity position, ft
α	angle of attack (in the vertical plane), deg
α_m	average value of maximum-angle envelope, $\frac{\alpha_{mi} + \alpha_{mf}}{2}$, deg
α_{mi}	initial value of maximum-angle envelope, deg (see sketch (a))
α_{min}	average value of minimum-angle envelope, $\frac{\alpha_{mini} + \alpha_{minf}}{2}$, deg
α_{mini}	initial value of minimum-angle envelope, deg (see sketch (a))
α_{mf}	value of maximum-angle envelope at end of flight, deg (see sketch (a))

$\alpha_{\min f}$	value of minimum-angle envelope at end of flight, deg (see sketch (a))
α_{rms}	root-mean-square angle of oscillation, $\sqrt{\frac{\int_0^x (\alpha^2 + \beta^2) dx}{x}}$, deg
β	angle of sideslip (in the horizontal plane), deg
Γ	static-stability parameter, $\frac{I}{\lambda^2 \rho A d}$, dimensionless
$\eta_{1,2}$	damping exponents in equation (1), ft ⁻¹
λ	wavelength of pitching oscillation, ft/cycle
ρ	free-stream air density, slugs/cu ft
σ	radius of gyration about a transverse axis through the center of gravity, ft
$\omega_{1,2}$	rates of rotation of vectors which describe the model pitching motion, radians/ft
$\frac{\omega d}{V}$	reduced frequency parameter, dimensionless
ξ	dynamic-stability parameter, $C_D - C_{L\alpha} + (C_{m\dot{q}} + C_{m\ddot{\alpha}})(d/\sigma)^2$, dimensionless
$(\dot{})$	first derivative with respect to time

MODELS AND TEST CONDITIONS

A comparison sketch of the Gemini and Mercury shapes is shown in figure 1. In full scale, the Gemini capsule is larger than the Mercury capsule; however, they are shown here superposed with the same maximum diameter to show the difference in blunt-face curvature and afterbody geometry, and the addition of window cutouts. Figure 2 is a detailed sketch of the Gemini model tested in the present investigation. The models were homogeneous; thus, the center of gravity was located at the center of volume, 0.52d from the blunt face. The axial location on the full-scale vehicle is 0.49d. Two sizes of models were used in the present investigation: the larger models, machined from phosphor bronze, had a 1.20-inch diameter; the smaller models, machined from 7075-T6 aluminum, had a 0.42-inch diameter. Figure 3 shows the two sizes of models used; both are models recovered after tests.

The models were gun-launched and time-distance histories and attitude histories were recorded at spark shadowgraph stations along the flight path. The larger models were launched from a 1.75-inch smooth-bore gun into still air at atmospheric pressure. The average velocity of the models in the test section was approximately 3300 ft/sec, corresponding to a Mach number of about 3. The nominal Reynolds number was 2.1×10^6 , based on free-stream conditions

~~CONFIDENTIAL~~

and model diameter. These tests were conducted in the Ames Pressurized Ballistic Range, which is equipped with 24 measuring stations along its 203-foot length.

The smaller models were launched from a 50-caliber smooth-bore gun into a Mach number 3 countercurrent air stream. The combined velocity of the model and air stream was approximately 6300 ft/sec, corresponding to a Mach number of about 9.5. The nominal Reynolds number was 1.4×10^6 , based on free-stream conditions and model diameter. These tests were conducted in the Ames Supersonic Free-Flight Wind Tunnel (ref. 4), which is instrumented with 9 measuring stations spaced at 3-foot intervals.

Because of the deceleration of the models, the Mach number and Reynolds number decreased uniformly with flight-path distance. Typical variations of these parameters encountered during the investigation are shown in figure 4. Figure 4(a) shows that the Mach number and Reynolds number decreased about 30 percent along the flight path of the models tested in the ballistic range at $M = 3$. Figure 4(b) shows that these parameters decreased about 20 percent along the flight path of the models tested in the free-flight wind tunnel at $M = 9.5$.

STABILITY DATA REDUCTION

Stability data were obtained from analyses of the attitude histories of the models. Examples of the pitching and yawing motions experienced by the models are shown in figure 5. The numbered symbols show the angles of attack and sideslip measured from the shadowgraphs at each of the stations. The curves are fitted to the data points by a method which will be discussed later. The data show precessing elliptical motions, with each flight differing in amount of precession (indicative of the model roll rate) and eccentricity. The majority of the flights exhibited nearly planar motion with little precession. Figures 5(a) and (b) are examples of this type of motion. Two of the tests at $M = 3$ and one at $M = 9.5$ showed less eccentricity and more precession as illustrated in figures 5(c) and (d).

To reduce the effects of Mach number and Reynolds number variations (fig. 4), the motions recorded in the $M = 3$ ballistic-range tests were analyzed in two parts, each part consisting of approximately 100 feet of flight and 2-1/2 cycles of oscillation. For example, the first half of the motion shown in figure 5(c) (stations 1 through 14) was analyzed as one flight, and the second half (stations 12 through 24) was treated as a separate motion. It was not possible to divide the trajectories from the wind-tunnel tests (figs. 5(b) and (d)) since these flights consisted of less than two cycles of oscillation.

To extract the static-stability parameter (ref. 5)

$$\Gamma = \frac{I}{\lambda^2 \rho A d}$$

~~CONFIDENTIAL~~

~~CONFIDENTIAL~~

and the dynamic-stability parameter (ref. 6)

$$\xi = C_D - C_{L\alpha} + (C_{m\dot{q}} + C_{m\dot{\alpha}})(d/\sigma)^2$$

from the attitude histories, the motion equation developed in reference 7 (further discussed in refs. 3 and 8) was used. Specifically, the tricyclic equation

$$\beta + i\alpha = K_1 e^{(\eta_1 + i\omega_1)x} + K_2 e^{(\eta_2 - i\omega_2)x} + K_3 e^{ipx} \quad (1)$$

was fitted by the method of least squares to the measured values of α and β for each flight. The exponents $\omega_{1,2}$ are related to the wavelength of oscillation by

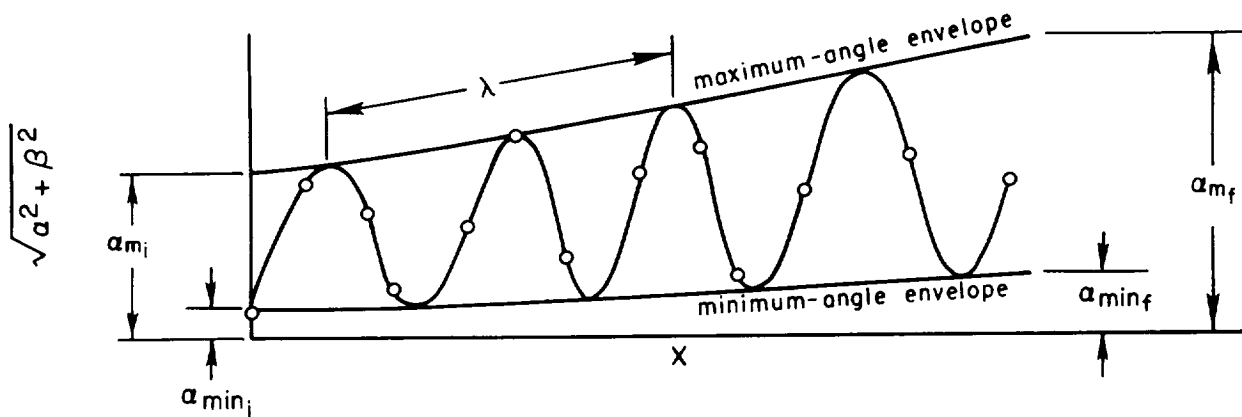
$$\lambda = \frac{2\pi}{\sqrt{\omega_1 \omega_2}}$$

and the exponents $\eta_{1,2}$ are related to ξ by

$$\xi = \frac{\eta_1 + \eta_2}{\rho A / 2m}$$

The curves in figure 5 show the best fits of equation (1) to the data and represent the motions very well.

To identify the amplitude of oscillation of each flight for presentation of the data, the minimum as well as the maximum angles of oscillation must be indicated because the angle range through which the models oscillated differed for each flight. These angles are defined in sketch (a).



$$\alpha_m = \frac{\alpha_{m_i} + \alpha_{m_f}}{2}; \quad \alpha_{\min} = \frac{\alpha_{\min_i} + \alpha_{\min_f}}{2}; \quad \alpha_{\text{rms}}^2 = \frac{1}{x} \int_0^x (\alpha^2 + \beta^2) dx$$

Sketch (a)

~~CONFIDENTIAL~~

RESULTS AND DISCUSSION

Experimental measurements of stability and drag of the Gemini entry models are summarized in table I along with other pertinent information. The Mach numbers and Reynolds numbers listed in the table are the average values for the flight or part of flight for which they are recorded. The angle range through which each model oscillated is indicated by the values of α_m , α_{min} , α_{m1} , and α_{rms} (see sketch (a)).

Static Stability

Nominal Mach number 3.— The experimental data for the present tests in terms of Γ versus $(\alpha_m^2 + \alpha_{min}^2)$ are shown in figure 6. In an effort to determine the effects of the window cutouts on the aerodynamic characteristics, two models without the cutouts were tested at Mach number 3. Data from these tests are shown as the filled symbols in figure 6. Unfortunately, these tests were both of low oscillation amplitude; however, the windows appear to have had no effect on the static stability at low angles of attack. The initial stability calculated from modified Newtonian impact theory is included in the figure and is seen to be about one-fourth of the experimental value. Two curves are shown for each set of data. The solid curve is the best fit of a quadratic equation to the data. The use of a quadratic equation results in a pitching moment which is linear plus cubic plus quintic in angle of attack. However, because of the lack of data in the region of $(\alpha_m^2 + \alpha_{min}^2)$ about 200, it was judged that the faired curves shown could equally well represent the variation of Γ .

Several suitable methods are available (refs. 9 to 12) for determining the nonlinear pitching-moment curves from the variations of the stability parameter shown in figure 6. The method of reference 12 was used to analyze the data from the present tests as well as the data from reference 3 for the Mercury capsule.

The pitching-moment curves corresponding to the curves shown in figure 6 are presented in figure 7. The effects of the differences between the fitted and faired curves of figure 6 are evident. Use of the faired curves increases the restoring moments and reduces the nonlinearities in the pitching-moment curves at angles of attack from 6° to 16° . This illustrates the uncertainty resulting from the insufficient data at large angles. Included in figure 7 are the curves for the Mercury capsule determined from the data reported in reference 3. Slightly different Mach number conditions are shown for the Mercury and Gemini configurations, but it can be seen that the Gemini capsule is the more statically stable of the two configurations at low angles of attack. This is attributed to the differences in afterbody flow as will be discussed later. In contrast to the Mercury configuration, the Gemini configuration shows an increase in static restoring moment with a decrease in Mach number and Reynolds number.

CONFIDENTIAL

Nominal Mach number 9.5. - The experimental data for the tests at $M = 9.5$ are shown in figure 8 which includes the result from one model at a Mach number of about 7.6. Also shown in the figure is the value at 0° angle of attack calculated by use of modified Newtonian impact theory. The predicted value is about one-third of that measured. The curve is the best fit of a quadratic equation to the data and represents quite well the measured variation of Γ . The data shown in figure 8 were obtained with models having no window cutouts. Launching difficulties were encountered in the tests at $M = 9.5$, and it was fortuitous that only windowless models were successfully launched. Therefore, it was not determined whether the window cutouts would affect the aerodynamic characteristics at this Mach number.

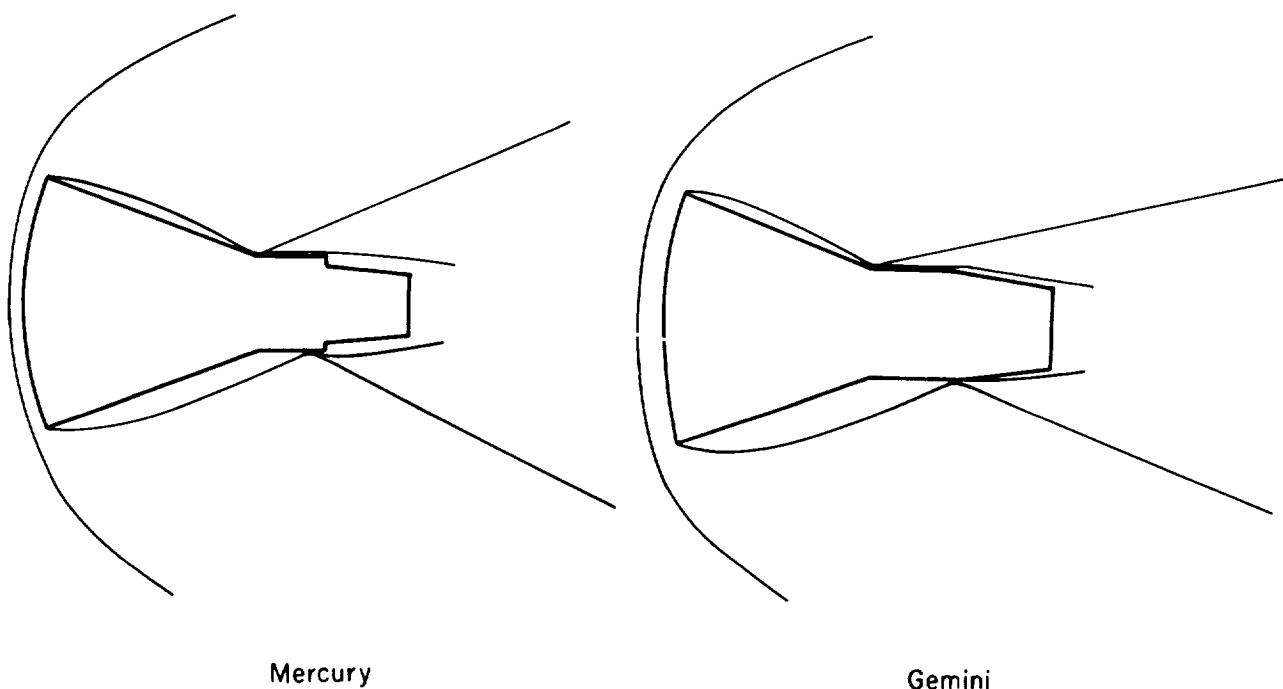
The pitching-moment curve corresponding to this variation is shown in figure 9, along with the curve deduced from the experimental data for the Mercury capsule at $M = 9.5$ (ref. 3). The results in reference 3 are for a more forward center-of-gravity position, $x_{cg} = 0.36d$. So to compare them with the results for the Gemini capsule, they were transferred to a moment center corresponding to the center of volume. To do this an experimental value was taken from reference 1 of the normal-force-curve slope ($C_{N\alpha} = 0.344$) for the Mercury capsule at $M = 9.5$. Both curves in figure 9 are highly nonlinear and are similar in shape, but the Gemini capsule is more stable throughout the angle range tested.

To summarize the results of the static-stability characteristics of the Gemini and Mercury configurations, values of the initial ($\alpha = 0$) moment-curve slopes are shown as a function of Mach number in figure 10. The Gemini configuration is statically more stable than the Mercury configuration at Mach numbers of 3.0 and 9.5, although, based on face curvature alone, the converse would be expected. Reference 13 shows that in the absence of an afterbody, the static stability decreases with a decrease in blunt-face curvature. However, it also shows that the afterbody contributes significantly to the static stability. In reference 13, the results for a Mercury type model without afterbody were compared to those from Mercury capsule tests (ref. 3). The Mercury model had more than twice the stability of the model without an afterbody. Thus, from a comparison of the Gemini and Mercury models, it appears that the contribution to static stability of the larger cylindrical part of the afterbody of the Gemini model more than compensates for the expected decrease in static stability caused by the smaller face curvature.

It can be seen in figure 10 that there is a larger difference in initial stability between the Gemini and Mercury configurations at $M = 3$ than at $M = 9.5$. This greater increase in initial stability of the Gemini capsule at $M = 3$ can probably be attributed to the differences in flow-field conditions over the afterbody of the Gemini and Mercury models which were not present at $M = 9.5$. A comparison of the shadowgraphs of the Gemini and Mercury models at low angles of attack is seen in figures 11(a) and (b) which show the models at a Mach number of 3.44. The flow over the afterbody of the Mercury model is completely separated, whereas the flow over the afterbody of the Gemini model appears to reattach in the vicinity of the cylindrical section and thus produces the stronger compression shocks observed. It can be seen that the separated region over the Gemini afterbody is thinner than that over the Mercury

afterbody. For a more direct comparison, figure 12 shows the profiles of the separated flow as measured from figures 11(a) and (b). This difference in flow conditions is undoubtedly due to the difference in face curvature and/or afterbody shape, but the quantitative effects of each were not determined. Figures 13(a) and (b) show the models at a Mach number of 9.8. It is difficult to see in these reproductions, but an examination of the original shadowgraphs showed that the flow conditions over the afterbody were very similar; that is, the flow separated at the corner but then reattached on the afterbody for both configurations (see sketch (b)).

Thus, the contrast in afterbody flow conditions between Gemini and Mercury at low angles of attack is greater at a Mach number of 3 than at 9.5. This correlates with the observation that the static stability difference between Gemini and Mercury models decreases with increasing Mach number.



Sketch (b)

Dynamic Stability

Nominal Mach number 3.— The results of dynamic-stability measurements for Gemini at a nominal Mach number of 3 are presented in figure 14, where the dynamic-stability parameter, ξ , is plotted as a function of the initial value of the maximum-angle envelope, α_{m1} . It can be seen that the model is dynamically unstable over the entire range tested for both Mach number and Reynolds number conditions. Included in the figure as filled symbols are the data for the models without window cutouts. The effect of the window cutouts on the

dynamic instability cannot be defined from these tests because of the scatter in the data at low amplitudes.¹ The flagged symbols in figure 14 are data from motions which were more circular, with minimum-to-maximum angle ratios, α_{\min}/α_m (see sketch (a)) greater than 0.3 as compared to approximately 0.1 or less for the other motions. It was shown in reference 3 that the measured value of ξ is a function of the angle range through which the models oscillate as well as the maximum angle of oscillation for configurations that exhibit nonlinear damping characteristics.

The same curve is faired through the data in figures 14(a) and (b) and is reproduced in figure 15 for comparison with the data for the Mercury configuration (ref. 3). The dynamic instability of the Gemini configuration decreases with increasing amplitude of oscillation; whereas, the Mercury data indicate a comparatively constant or slightly increasing dynamic instability with increasing amplitude.

Nominal Mach number 9.5.— The dynamic-stability results for the Gemini configuration at a Mach number of 9.5 are presented in figure 16. The results show the dynamic-stability parameter to be nearly constant for angles of oscillation greater than about 6° . Included in the figure are the data reproduced from reference 3 for the Mercury capsule. As noted, the Mercury data are for a more forward center-of-gravity location. It is shown in reference 3 that at $M = 3$, the dynamic instability increased with a rearward movement of the center of gravity. If this also occurs at $M = 9.5$, the effect would be to shift the curve for the Mercury data in figure 16 toward closer agreement with the data for the Gemini capsule. Because of lack of data for the Gemini capsule at low amplitudes of oscillation, it cannot be determined whether the Gemini capsule would exhibit a highly unstable region at low angles of attack, as indicated by the trend of the Mercury data.

Also included in figure 16 is the value of ξ obtained for the Gemini capsule at a Mach number of 7.6. A comparison with the data in figure 14 shows that at amplitudes of about 16° there is little effect of Mach number on ξ for the Gemini capsule.

Drag

Drag coefficients were computed from the deceleration of the models by the procedure described in reference 14. The results are shown in figure 17, where C_D is plotted as a function of the mean-squared angle of attack. Drag coefficients for the Mercury capsule are not included in the figure because values of α_{rms} are not tabulated in reference 3. The drag of the Gemini capsule, however, is approximately 2 percent higher than the drag of the Mercury capsule at both Mach number conditions.

¹Experimental errors in measuring α and β have a large effect on ξ in tests of low amplitude oscillation, since the error in ξ is proportional to the percentage error in amplitude which increases as the amplitude decreases.

In figure 17(a), each data point represents a complete flight, since the Mach 3 tests were not divided into two parts for determining drag coefficients as they were for stability analysis. Therefore, only one value for C_D and α_{rms} is listed in table I for each flight at a nominal Mach number of 3. Included in figure 17 are the values of C_D calculated by use of modified Newtonian impact theory. The theory overestimates the drag by about 5 percent at both Mach numbers.

Lift

A limited amount of data on the lift characteristics of Gemini was obtained. Only when the model produced a definable swerve trajectory could a value be determined for the lift-curve slope, $C_{L\alpha}$. There was insufficient swerve in the trajectories of the models launched in the ballistic range to obtain data on the lift characteristics at $M = 3$. The models used in the wind-tunnel tests at $M = 9.5$ were light weight and produced adequate swerve for analysis. Four of these flights were investigated and the values of $C_{L\alpha}$ obtained are listed in table I. It can be seen that the four values agree with one another reasonably well. Modified Newtonian impact theory predicts a value of -1.65 which overestimates the measured values by about 35 percent.

Summary of Results

The following table summarizes the comparison of the aerodynamic characteristics of the Gemini entry capsule with the Mercury entry capsule for the center of gravity located at the center of volume. The data for the Mercury capsule were obtained from references 1, 2, and 3. The values in the first four columns have been previously discussed. The values of the damping-in-pitch derivative, $C_{mq} + C_{m\dot{\alpha}}$, were calculated from

$$\xi = C_D - C_{L\alpha} + (C_{mq} + C_{m\dot{\alpha}}) \left(\frac{\dot{\alpha}}{\sigma} \right)^2$$

Even when the values of $C_{mq} + C_{m\dot{\alpha}}$ are negative, the values of ξ are positive; thus, the destabilizing effect of the high drag and negative lift-curve slope overshadows the stabilizing effect of the damping-in-pitch derivatives.

~~CONFIDENTIAL~~

M = 3					
	$\frac{C_{m\alpha}}{\frac{x_{cg}}{d}} = 0.52$ $\alpha = 0$	ξ $\alpha = 2^\circ \text{ to } 16^\circ$	C_D $\alpha = 0$	$C_{L\alpha}$ $\alpha = 0$	$C_{mq} + C_{m\dot{\alpha}}$ $\alpha = 2^\circ \text{ to } 16^\circ$
Mercury	-0.27	2 to 6	1.56	-1.2	-0.1 to +0.5
Gemini	-.37	6 to 2	1.59	---	---
M = 9.5					
Mercury	-0.22	5 to 1	1.57	-1.2	+0.3 to -0.3
Gemini	-.24	--- to 2	1.62	-1.3	--- to -0.2

Other results of this investigation can be summarized as follows:

1. With the center of gravity located at the center of volume, both configurations are statically stable and dynamically unstable at both Mach numbers and at amplitudes of oscillation up to 16° .
2. The Gemini capsule exhibits more static stability than does the Mercury capsule. Nonlinearities are present in the pitching-moment curves for both configurations. At the lower Mach number there are differences in flow-field conditions over the afterbodies of the two capsules but with an increase in Mach number the flows become more similar.
3. Values of the dynamic-stability parameter range from about 1 to 6 for both configurations. At a Mach number of 3, the dynamic instability of the Gemini capsule decreases with increasing amplitude of oscillation; whereas, the dynamic instability of the Mercury capsule is comparatively constant or increases slightly with amplitude. At a Mach number of 9.5, the dynamic instability of the Gemini capsule is nearly constant at amplitudes of oscillation greater than about 6° .
4. The small changes in shape from the Mercury to the Gemini capsule increase the drag about 2 percent at both Mach numbers and increase the magnitude of negative lift-curve slope at $M = 9.5$.
5. For both configurations in free flight, the dynamically stabilizing effect of the damping-in-pitch derivatives is overshadowed by the destabilizing effect of the high drag and negative lift-curve slope.

Ames Research Center
National Aeronautics and Space Administration
Moffett Field, Calif., Jan. 6, 1964

~~CONFIDENTIAL~~

CONFIDENTIAL

REFERENCES

1. NASA Space Task Group: Static Longitudinal Stability Characteristics of the Mercury Capsule Configurations $M = 0.05$ to 20 . NASA Project Mercury Working Paper No. 124, March 18, 1960.
2. NASA Space Task Group: Summary of Dynamic Stability Data for the Mercury Capsule and Escape System. NASA Project Mercury Working Paper No. 186, March 22, 1961.
3. Sommer, Simon C., Short, Barbara J., and Compton, Dale L.: Free-Flight Measurements of Static and Dynamic Stability of Models of the Project Mercury Reentry Capsule at Mach Numbers 3 and 9.5. NASA TM X-373, 1960.
4. Seiff, Alvin: A Free-Flight Wind Tunnel for Aerodynamic Testing at Hypersonic Speeds. NACA Rep. 1222, 1955.
5. Whiting, Ellis E.: An Exploratory Investigation of Fins as Stabilizers for Blunt-Nosed Slender Bodies at Hypersonic Speeds. NASA TM X-657, 1962.
6. Allen, H. Julian: Motion of a Ballistic Missile Angularly Misaligned With the Flight Path Upon Entering the Atmosphere, and Its Effect Upon Aerodynamic Heating, Aerodynamic Loads, and Miss Distance. NACA TN 4048, 1957.
7. Nicolaidis, John D.: On the Free-Flight Motion of Missiles Having Slight Configurational Asymmetries. BRL Rep. 858, Aberdeen Proving Ground, 1953.
8. Short, Barbara J., and Sommer, Simon C.: Some Measurements of the Dynamic and Static Stability of Two Blunt-Nosed, Low-Fineness-Ratio Bodies of Revolution in Free Flight at $M = 4$. NASA TM X-20, 1959.
9. Kirk, Donn B.: A Method for Obtaining the Nonlinear Aerodynamic Stability Characteristics of Bodies of Revolution From Free-Flight Tests. NASA TN D-780, 1961.
10. Rasmussen, Maurice L.: Determination of Nonlinear Pitching-Moment Characteristics of Axially Symmetric Models from Free-Flight Data. NASA TN D-144, 1960.
11. Murphy, Charles H.: The Measurement of Nonlinear Forces and Moments by Means of Free-Flight Tests. BRL Rep. 974, Aberdeen Proving Ground, 1956.
12. Kryloff, N., and Bogoliuboff, N. (Solomon Lefschetz, trans.): Introduction to Nonlinear Mechanics. Annals of Mathematical Studies, no. 11, Princeton Univ. Press, 1943.

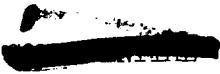
- 
13. Intrieri, Peter F.: Effects of Transverse Center-of-Gravity Displacement, Afterbody Geometry, and Front-Face Curvature on the Aerodynamic Characteristics of Mercury-Type Models at a Mach Number of 5.5. NASA TM X-569, 1961.
 14. Seiff, Alvin: A New Method for Computing Drag Coefficients from Ballistic Range Data. Jour. Aero. Sci., vol. 25, no. 2, Feb. 1958, pp. 133-134.

TABLE I.- EXPERIMENTAL CONDITIONS AND DATA

Test no.	M	$R \times 10^{-6}$	V, ft/sec	$\rho \times 10^3$, slugs/ft ³	$\Gamma \times 10^2$	σ_m , deg	σ_{min} , deg	ξ	σ_{mi} , deg	C_D	σ_{rms} , deg	$C_{L\alpha}$, per radian	λ , ft/cycle	$\frac{\omega d}{V}$	$\frac{x_{cg}}{d}$	d, in.	$(\frac{d}{\sigma})^2$	$m \times 10^3$, slugs	$\Gamma \times 10^5$, slug-ft ²
Nominal Mach number of 3																			
574-1	3.28	2.28	3690	2.349	0.415	4.17	1.51	7.02	3.41	1.59	3.64	---	45.8	0.0137	0.520	1.199	5.00	8.053	1.61
574-2	2.75	1.92	3100	2.349	.410	5.45	1.99	2.32	5.12	---	---	---	46.1	.0136	.520	1.199	5.00	8.053	1.61
575-1	3.31	2.25	3740	2.304	.446	3.38	0.32	4.24	2.86	1.59	2.83	---	44.7	.0140	.520	1.199	5.00	8.060	1.61
575-2	2.78	1.89	3140	2.304	.456	4.30	.28	5.69	3.58	---	---	---	44.2	.0142	.520	1.199	5.00	8.060	1.61
576-1	3.35	2.32	3780	2.334	.357	8.31	.58	3.25	7.50	1.58	6.47	---	49.6	.0126	.520	1.199	4.99	8.043	1.61
576-2	2.81	1.95	3180	2.334	.384	9.88	1.14	2.96	9.08	---	---	---	47.9	.0131	.520	1.199	4.99	8.043	1.61
a577-1	3.36	2.32	3790	2.325	.425	3.88	0.59	1.12	3.77	1.59	3.05	---	45.3	.0139	.517	1.200	5.00	8.058	1.61
a577-2	2.81	1.94	3170	2.325	.450	4.47	1.06	3.77	3.90	---	---	---	44.3	.0142	.517	1.200	5.00	8.058	1.61
a582-1	3.19	2.24	3610	2.366	.488	3.52	.22	4.62	2.99	---	---	---	42.5	.0149	.515	1.199	5.03	8.109	1.61
a582-2	2.67	1.87	3010	2.366	.488	3.52	.22	4.62	2.99	---	---	---	42.2	.0149	.515	1.199	5.03	8.109	1.61
583-1	3.23	2.29	3630	2.385	.420	4.52	.15	3.19	4.16	1.59	3.75	---	45.4	.0138	.518	1.199	4.97	8.065	1.62
583-2	2.70	1.91	3030	2.385	.408	5.65	.38	4.21	4.84	---	---	---	46.1	.0136	.518	1.199	4.97	8.065	1.62
584-1	3.09	2.16	3490	2.349	.440	4.52	.25	5.77	3.83	1.59	3.83	---	44.7	.0140	.518	1.200	5.01	8.119	1.62
584-2	2.59	1.80	2910	2.349	.428	6.03	.32	5.04	5.04	---	---	---	45.3	.0139	.518	1.200	5.01	8.119	1.62
585-1	3.29	2.31	3700	2.370	.275	16.16	.34	1.78	15.26	1.55	12.12	---	56.1	.0112	.516	1.200	5.00	8.053	1.61
585-2	2.76	1.94	3110	2.370	.308	17.88	.74	2.16	16.75	---	---	---	53.1	.0118	.516	1.200	5.00	8.053	1.61
Nominal Mach number of 9.5																			
a1116	7.57	1.11	5080	0.946	0.212	15.82	0.74	1.94	14.54	1.55	11.33	---	19.9	0.0110	0.513	0.419	4.98	1.081	2.64
a1125	9.73	1.33	6720	.904	.195	17.43	.29	1.86	16.47	1.58	12.06	-1.14	21.0	.0104	.512	.420	5.06	1.089	2.63
a1140	8.88	1.34	5920	.959	.205	14.88	3.44	2.37	13.28	1.56	10.67	-1.30	20.0	.0110	.512	.420	5.02	1.091	2.67
a1156	9.43	1.32	6440	.914	.284	6.40	1.22	1.44	6.13	1.62	4.61	-1.26	17.3	.0127	.514	.420	5.11	1.091	2.62
a1160	9.54	1.41	6400	.951	.230	11.39	1.54	1.41	10.92	1.59	7.73	-1.29	18.8	.0117	.511	.421	5.09	1.088	2.62

aDesignates models with no window cutouts.

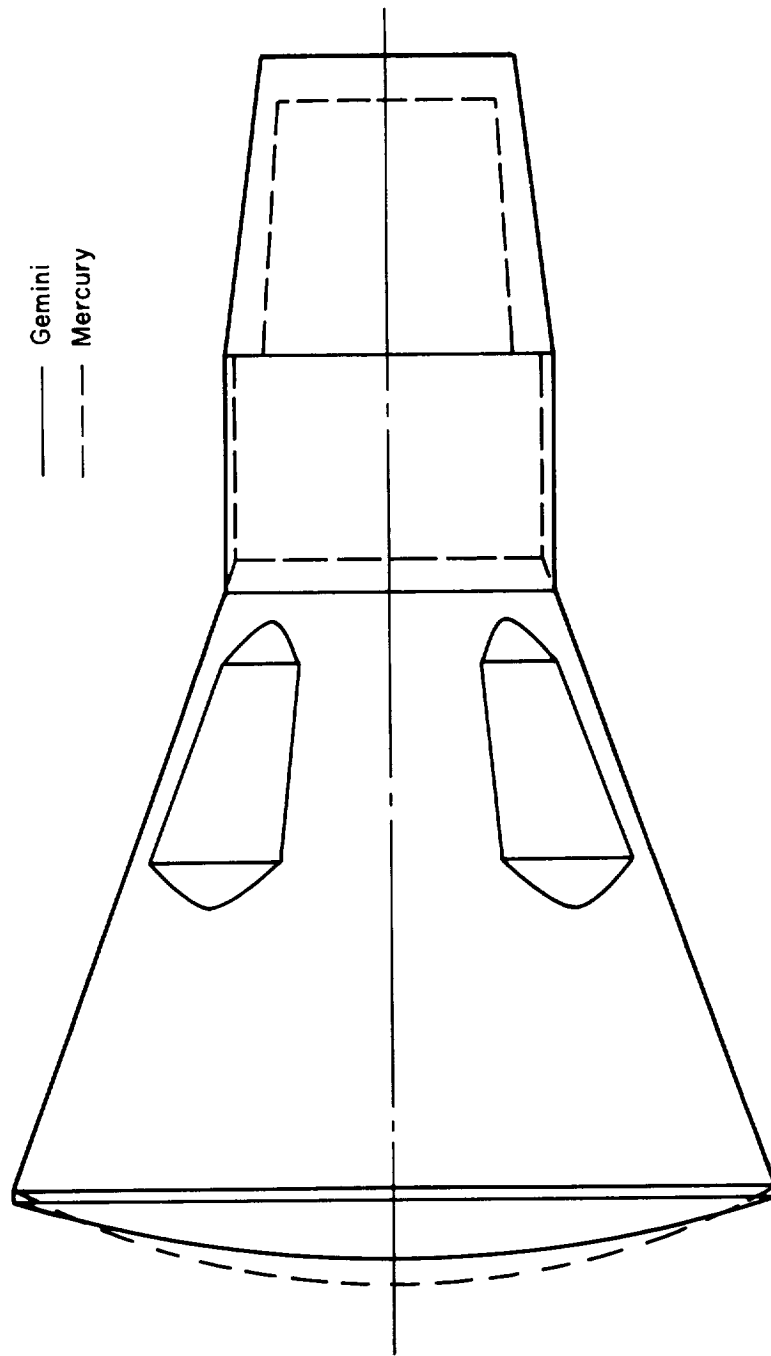
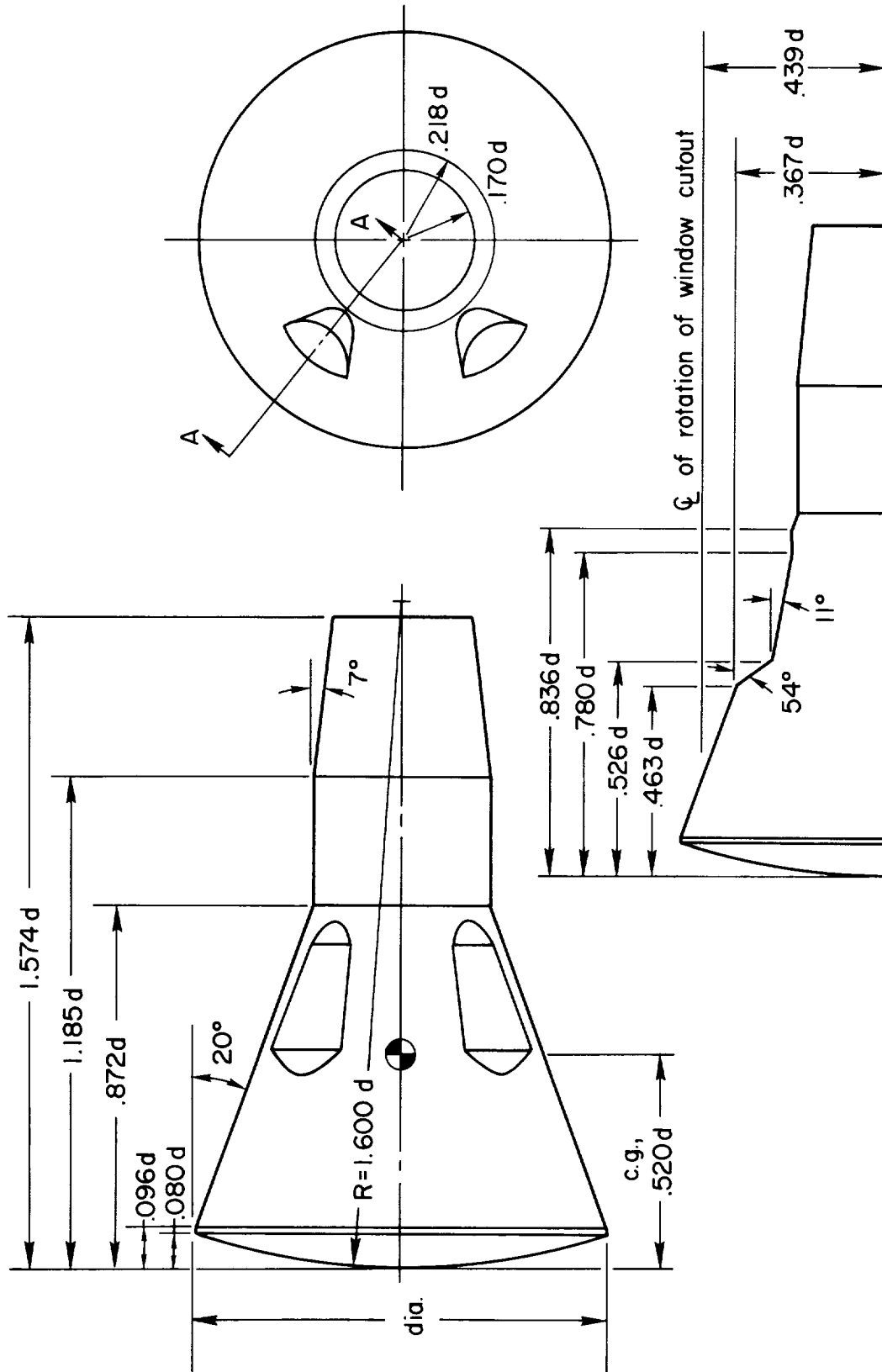
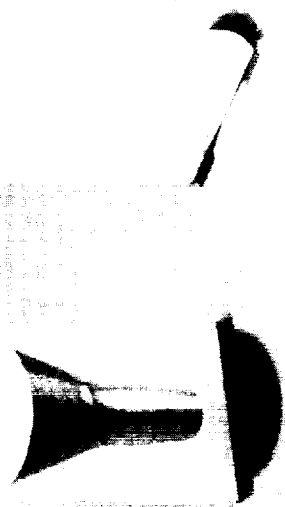
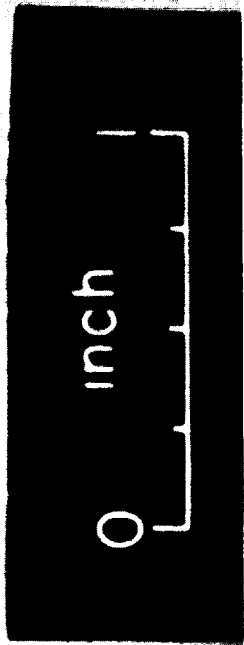
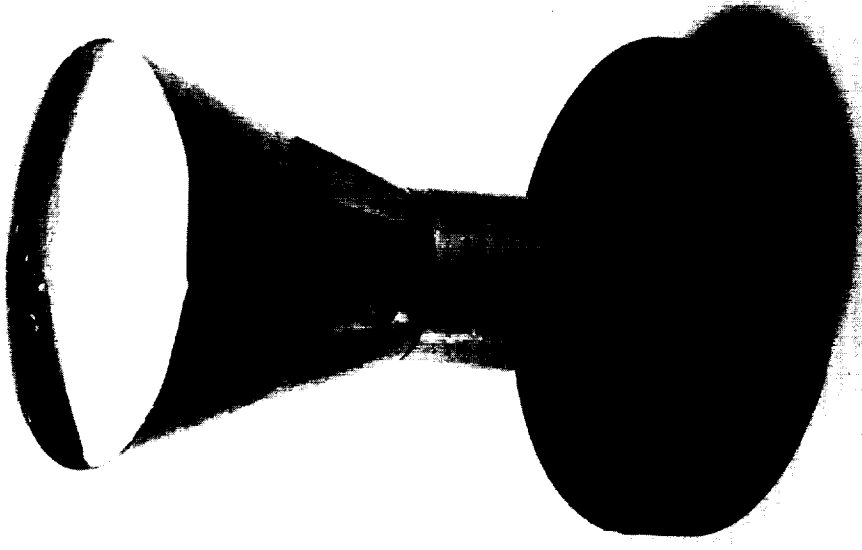


Figure 1.- Comparison sketch of Gemini and Mercury.



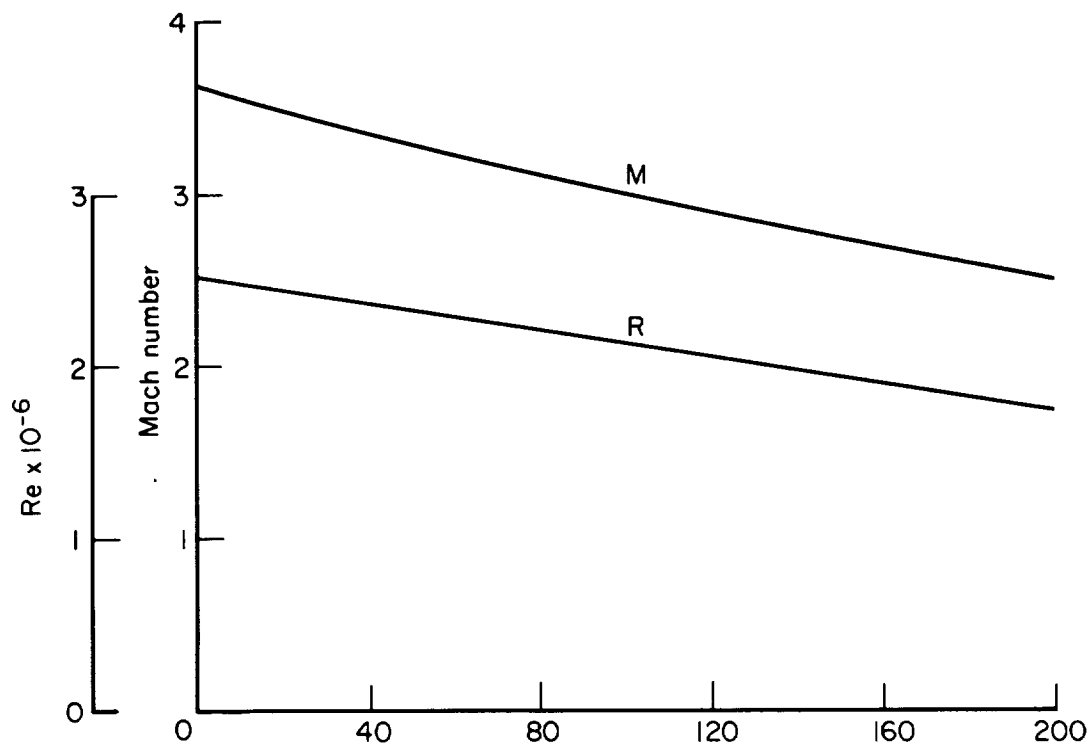
Section A-A, window cutout detail

Figure 2.- Sketch of Gemini model.

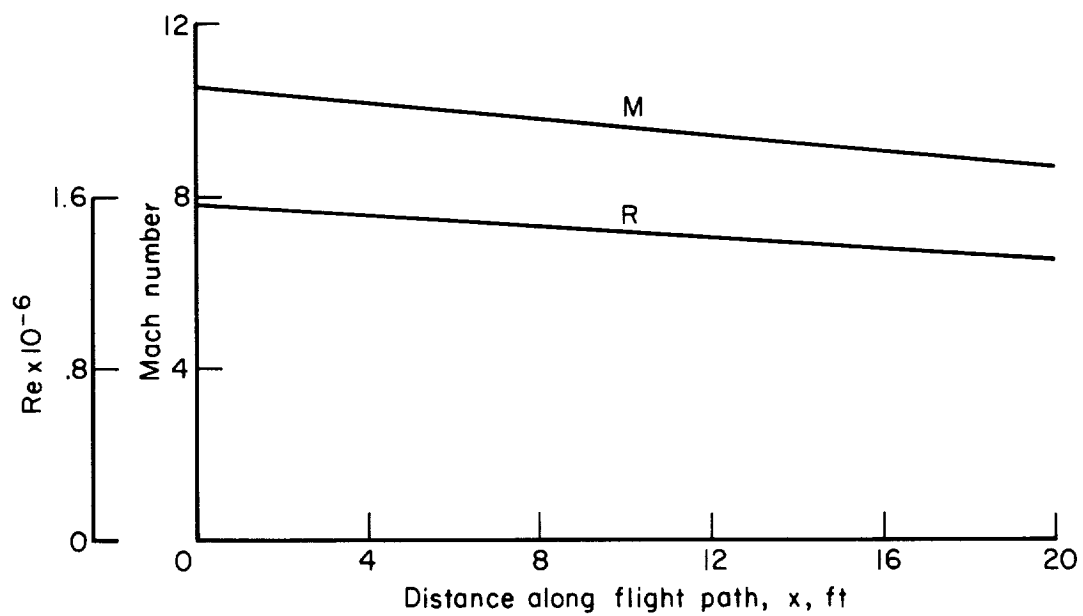


A-31220

Figure 3.- Models and sabot.

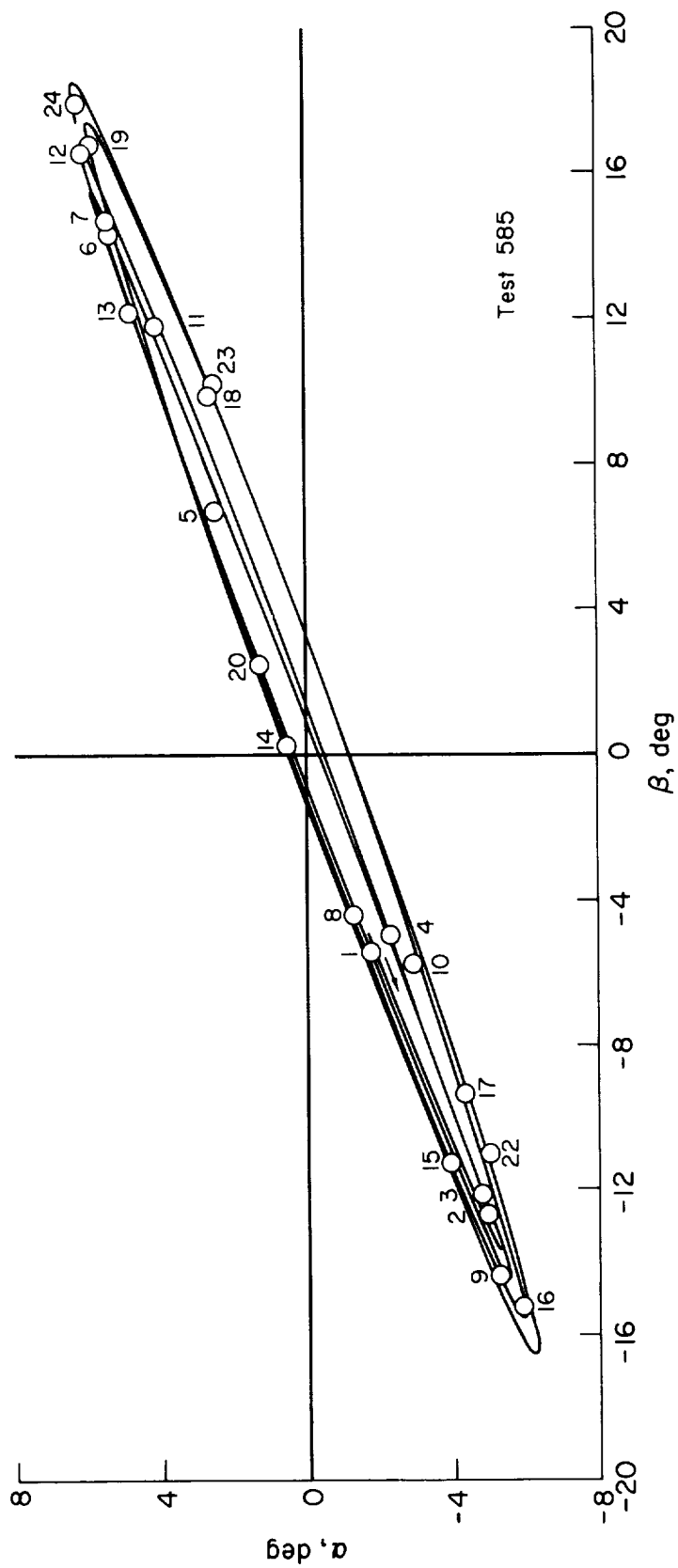


(a) Ballistic-range tests.



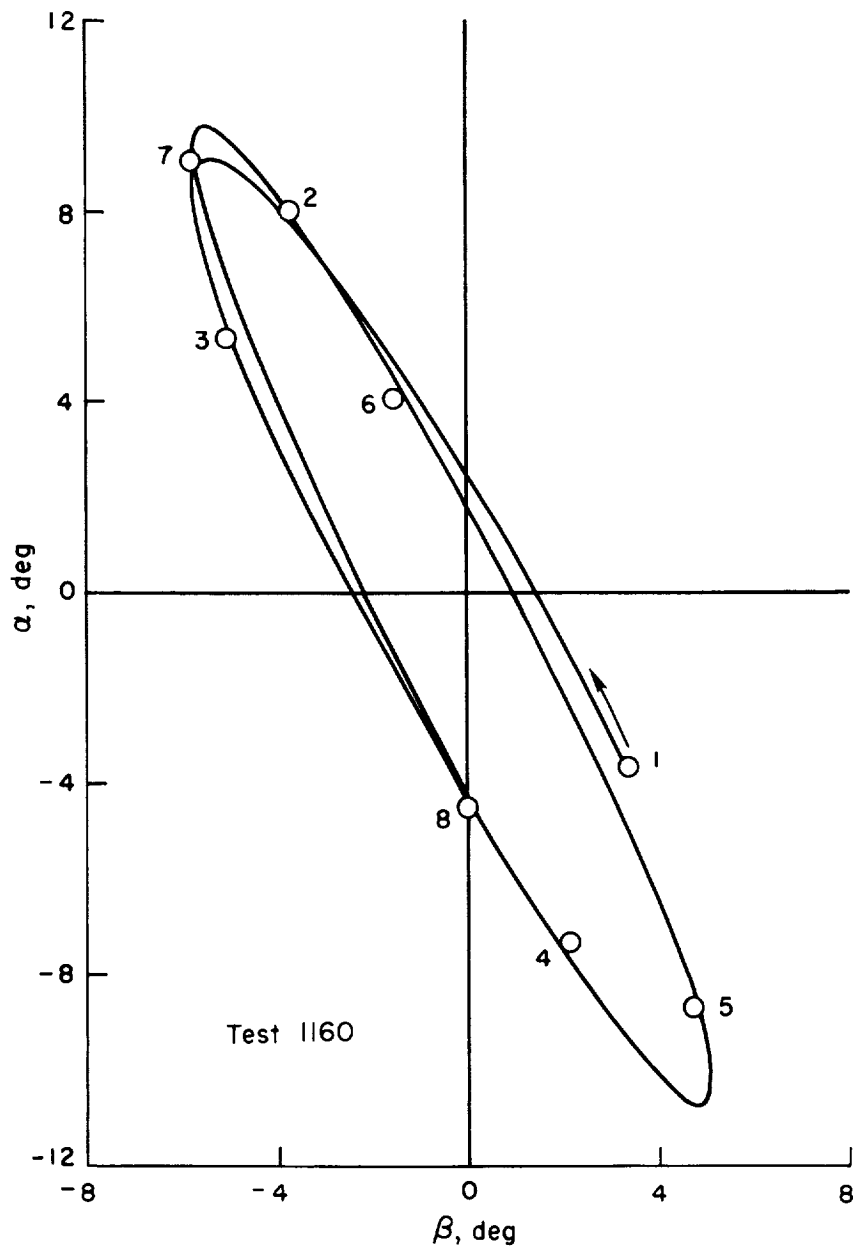
(b) Wind-tunnel tests.

Figure 4.- Typical Mach number and Reynolds number variations.



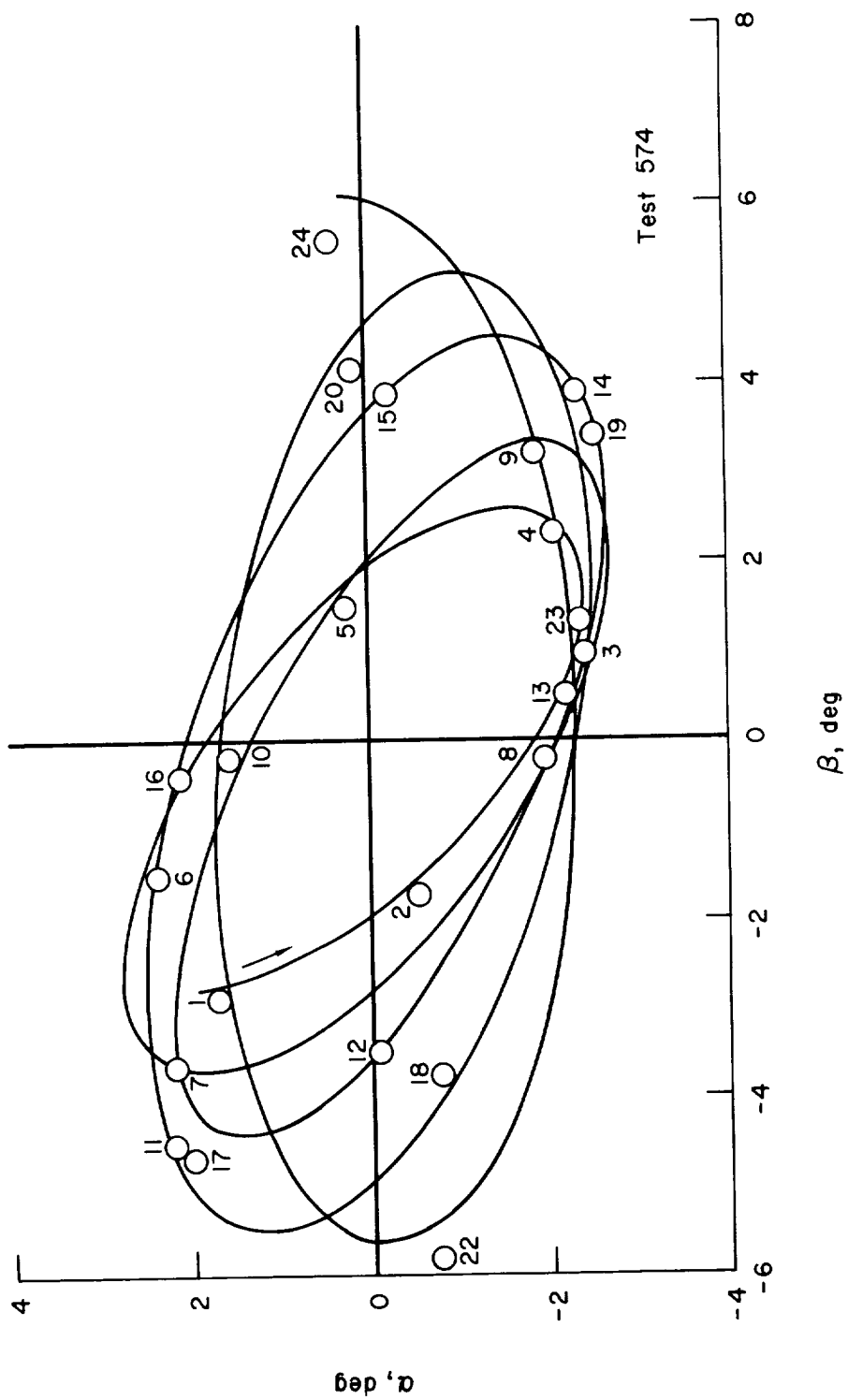
(a) $M \approx 3$ (ballistic-range test), high eccentricity.

Figure 5.- Typical pitching and yawing motions.



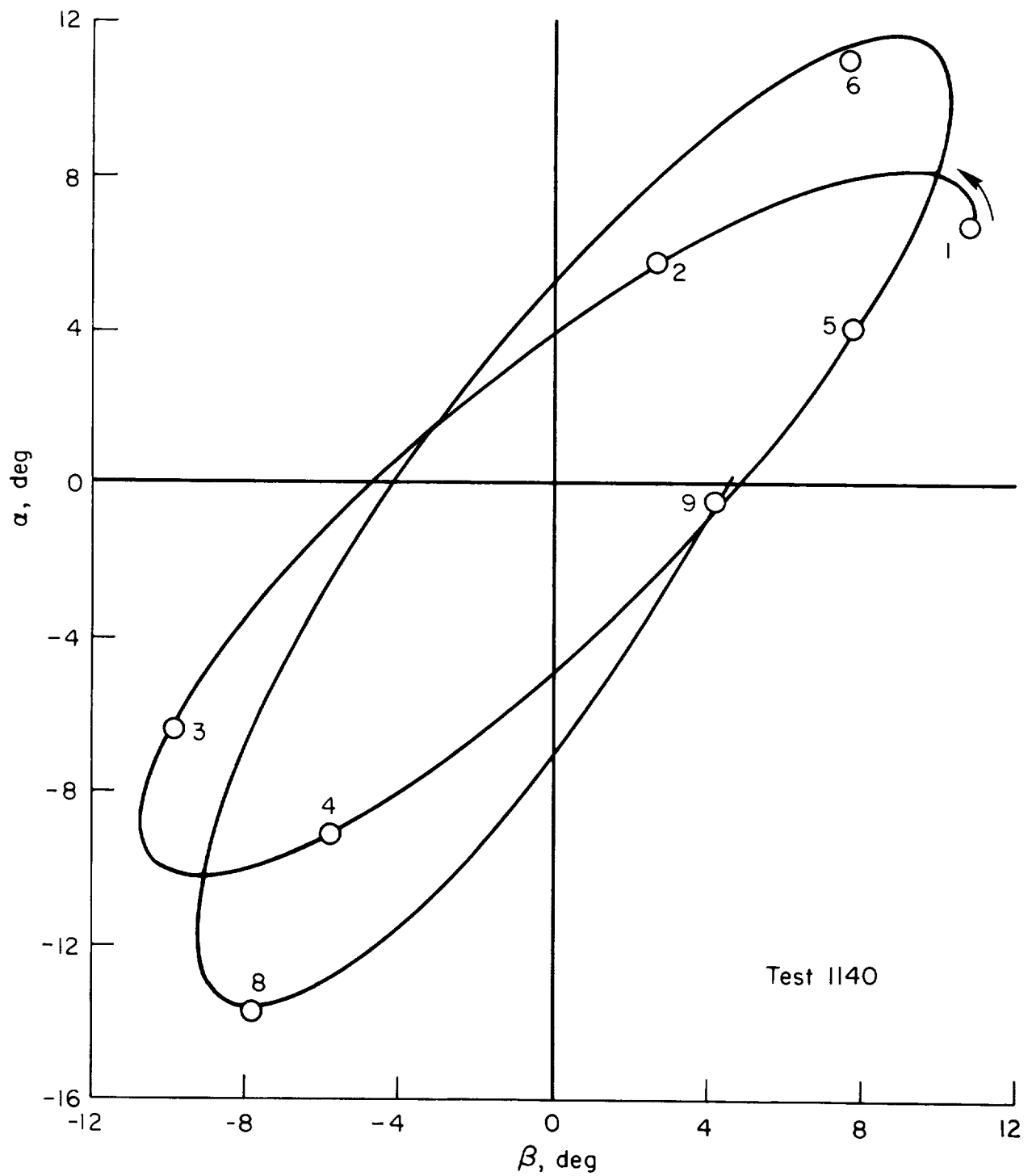
(b) $M \approx 9.5$ (wind-tunnel test), high eccentricity.

Figure 5.- Continued.



(c) $M \approx 3$ (ballistic-range test), low eccentricity.

Figure 5.- Continued.



(d) $M \approx 9.5$ (wind-tunnel test), low eccentricity.

Figure 5.- Concluded.

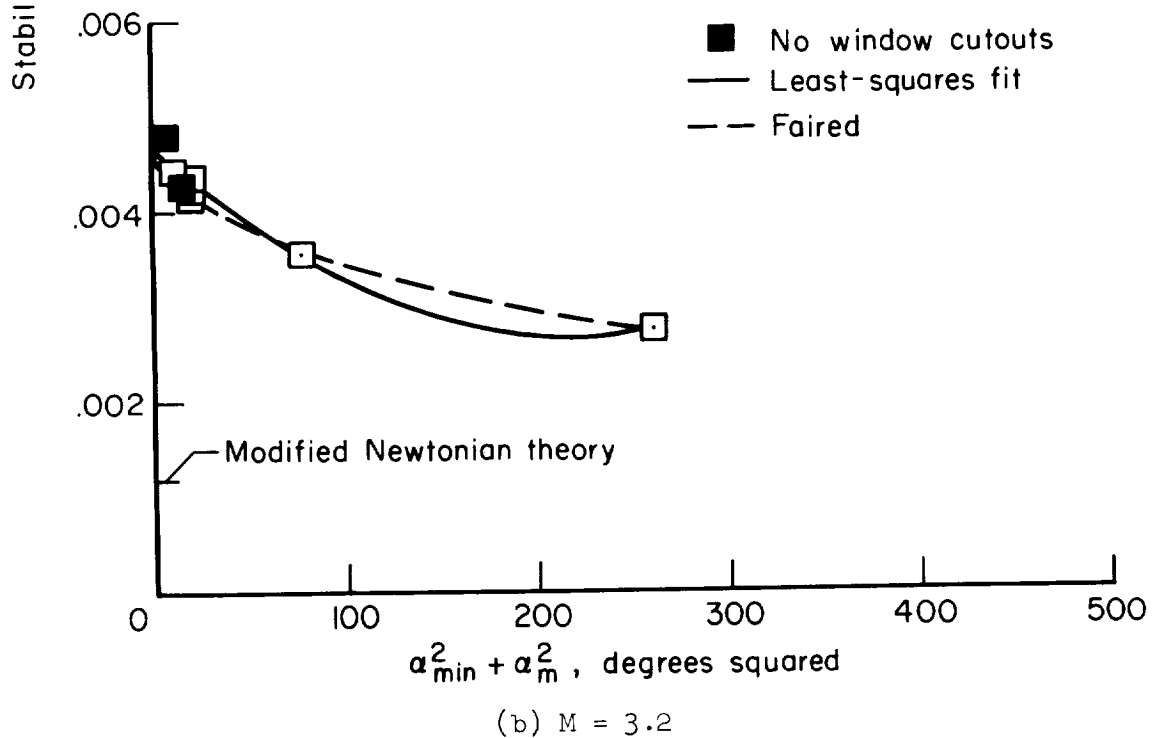
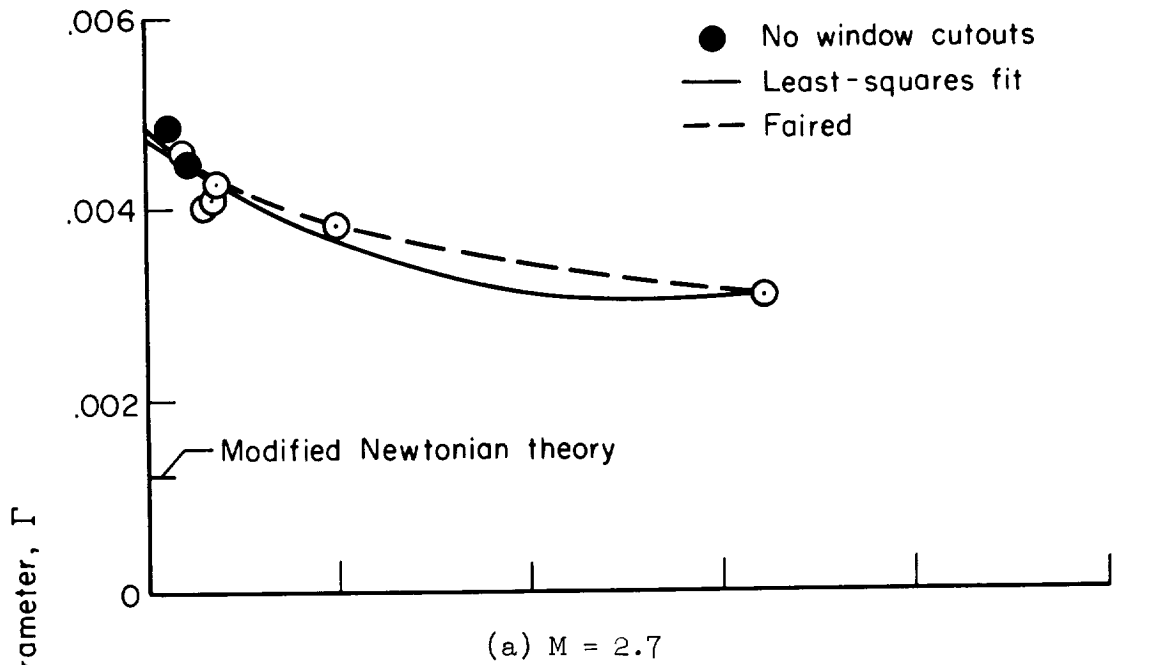


Figure 6.- Variation of static stability parameter with $(\alpha_{\min}^2 + \alpha_m^2)$ for nominal Mach number of 3.

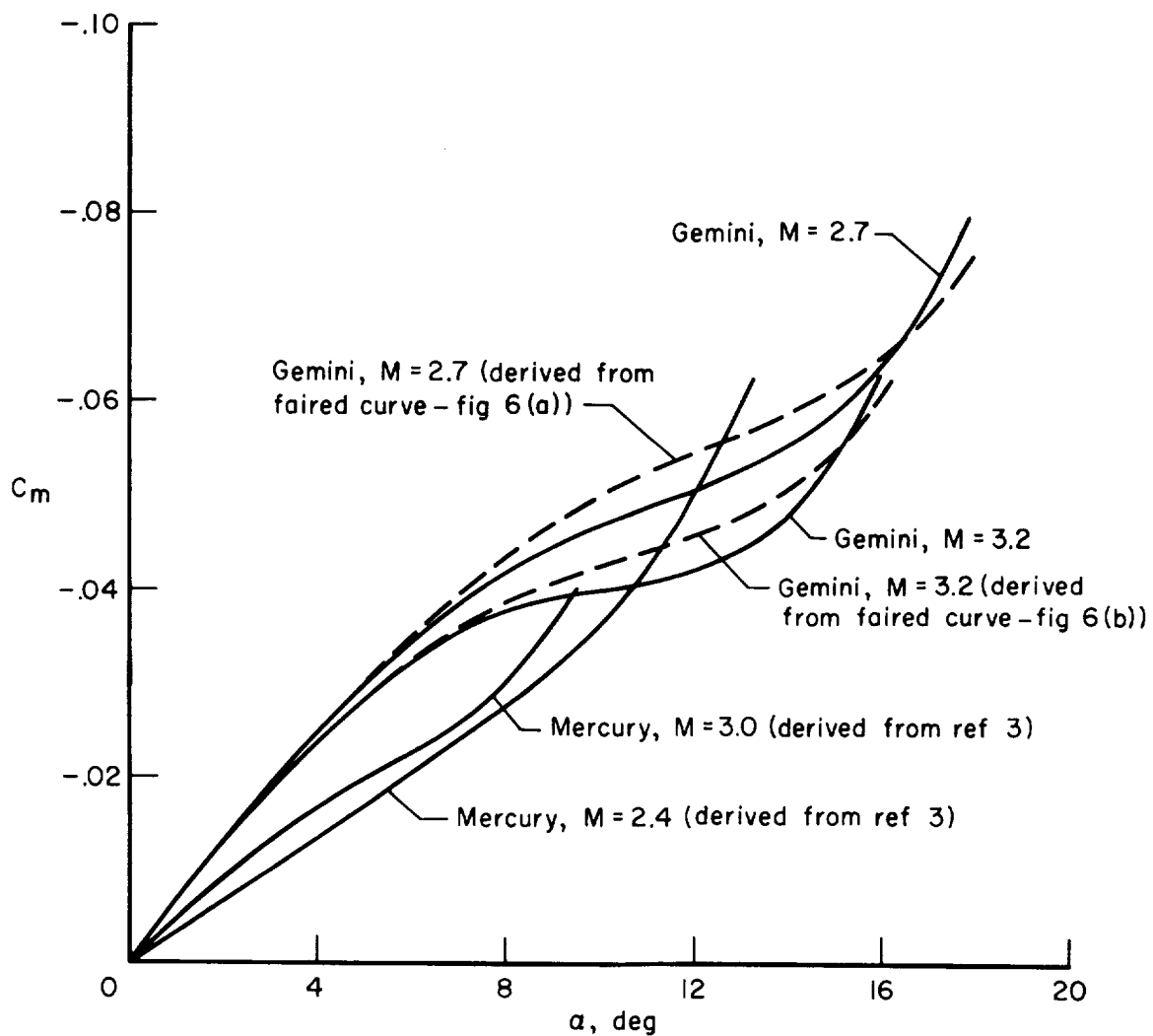


Figure 7.- Comparison of Gemini and Mercury pitching-moment coefficients at a nominal Mach number of 3.

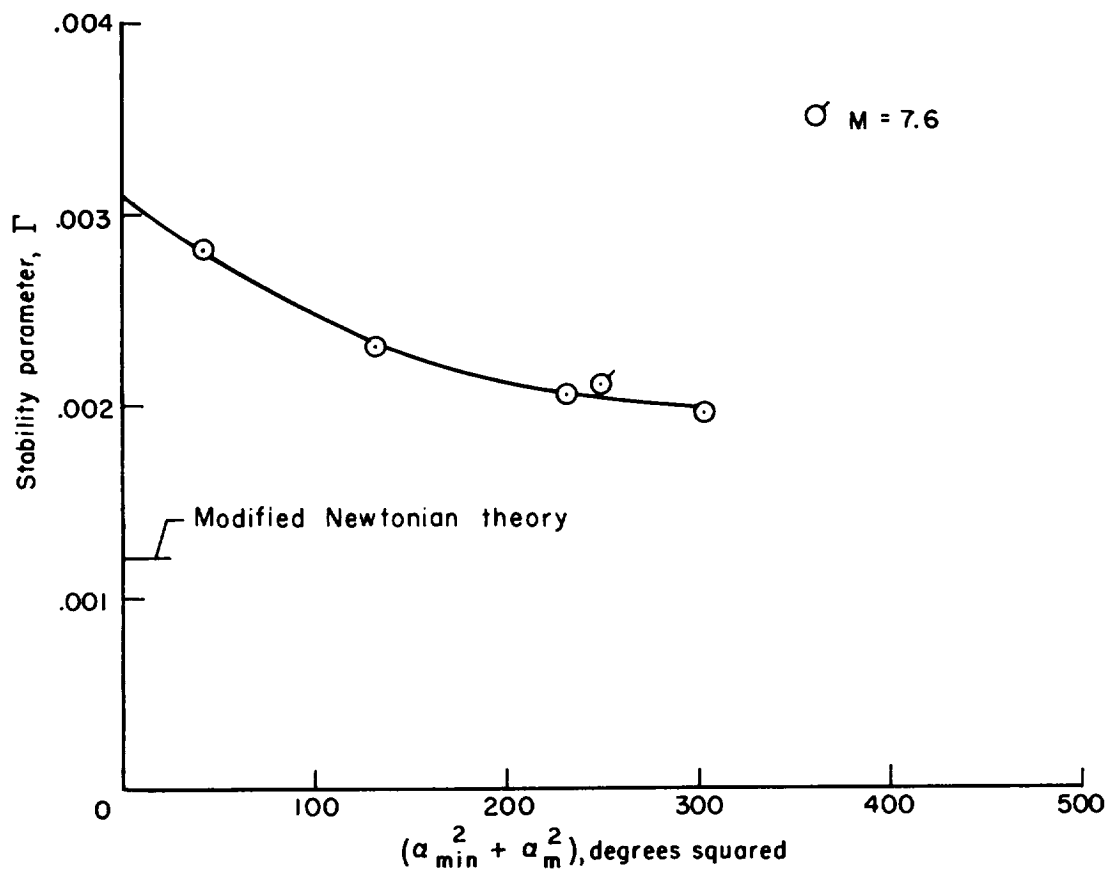


Figure 8.- Variation of static stability parameter with $(\alpha_{min}^2 + \alpha_m^2)$ for a nominal Mach number of 9.5.

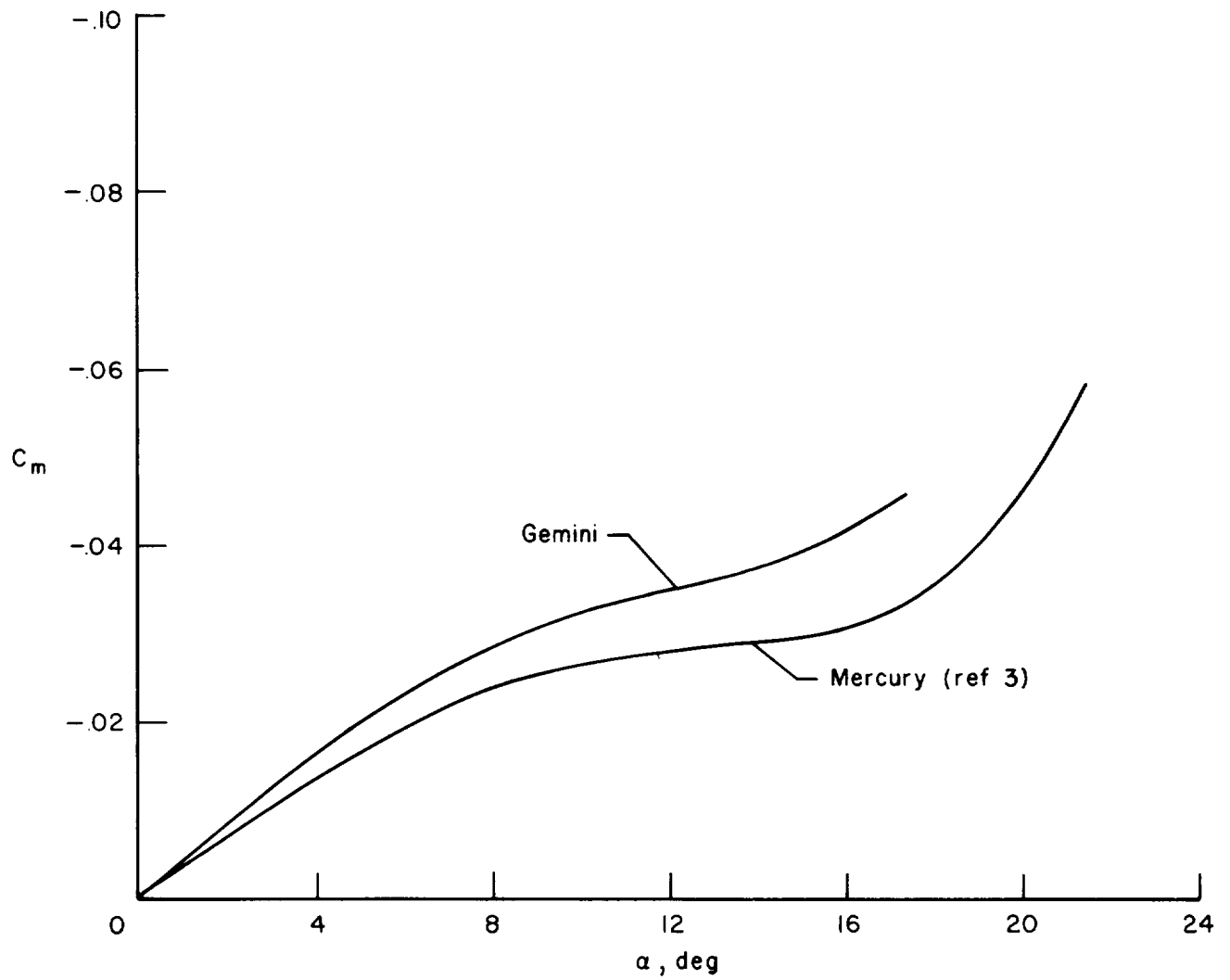


Figure 9.- Comparison of pitching-moment coefficients for Gemini and Mercury at a nominal Mach number of 9.5.

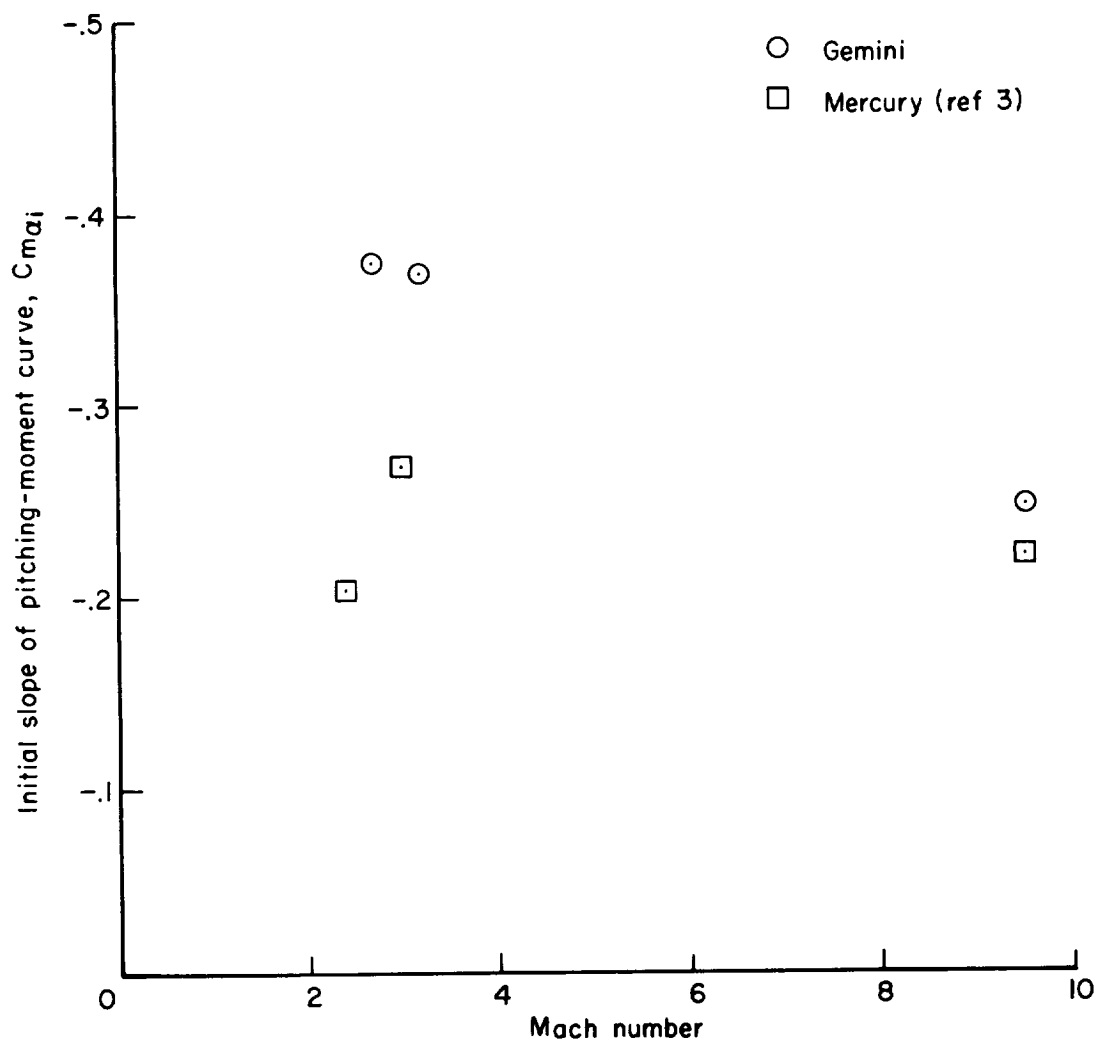
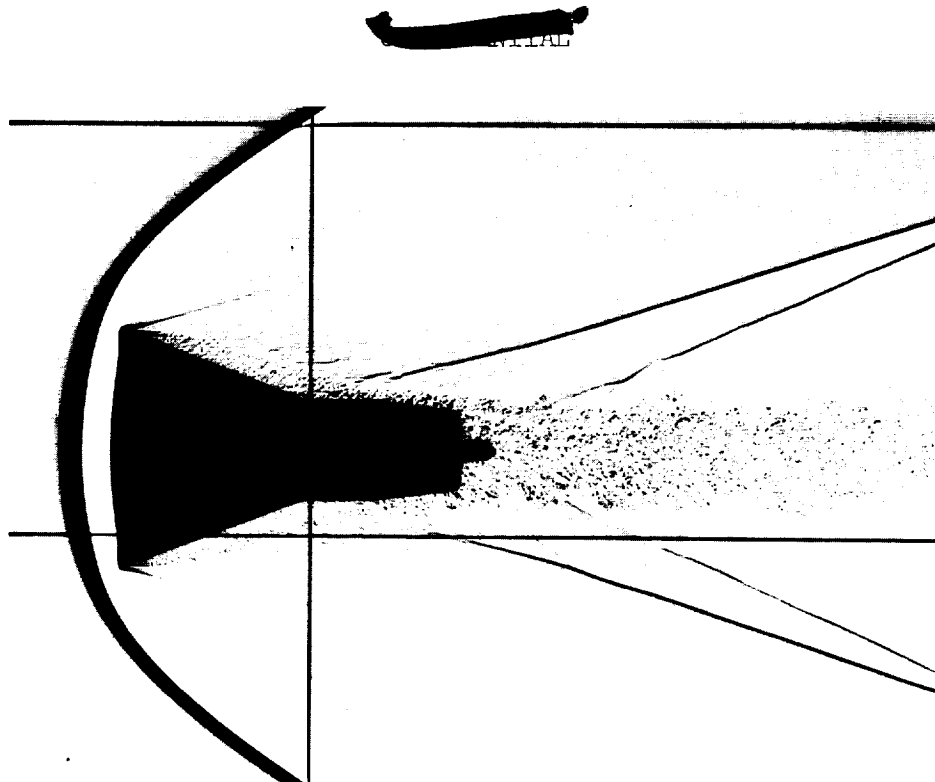
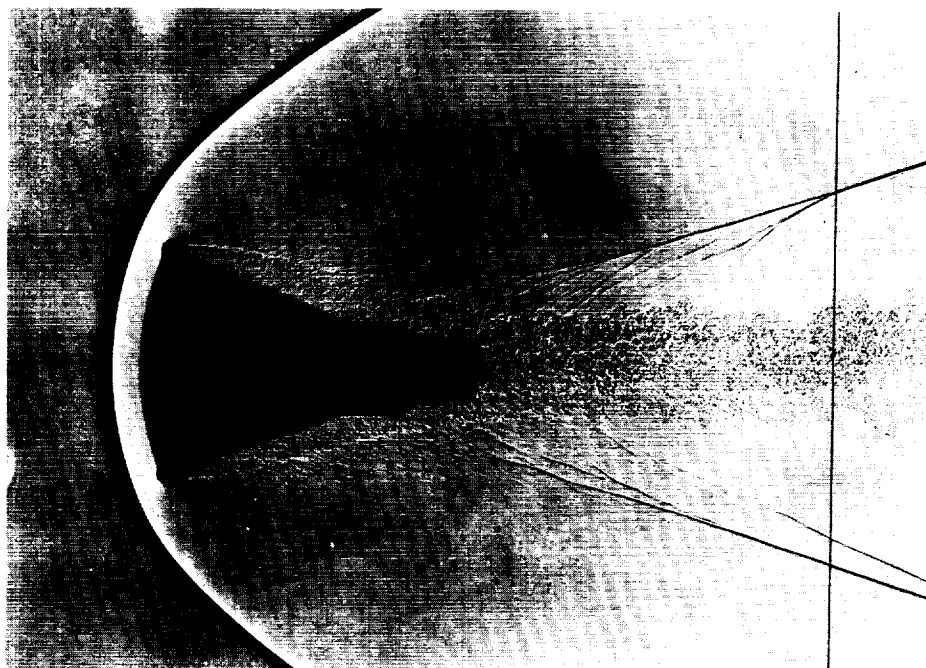


Figure 10.- Initial slope of pitching-moment curve versus Mach number for Gemini and Mercury tests.



A-30527

(a) Gemini (ballistic-range test), $\alpha = 0.0^\circ$ ($\beta = 0.4^\circ$), $M = 3.44$, $R = 2.4 \times 10^6$.



A-25027

(b) Mercury (ballistic-range test), $\alpha = 0.7^\circ$, ($\beta = 0.9^\circ$), $M = 3.44$, $R = 2.62 \times 10^6$.

Figure 11.- Typical shadowgraphs at $M = 3$.

— Gemini
- - - Mercury

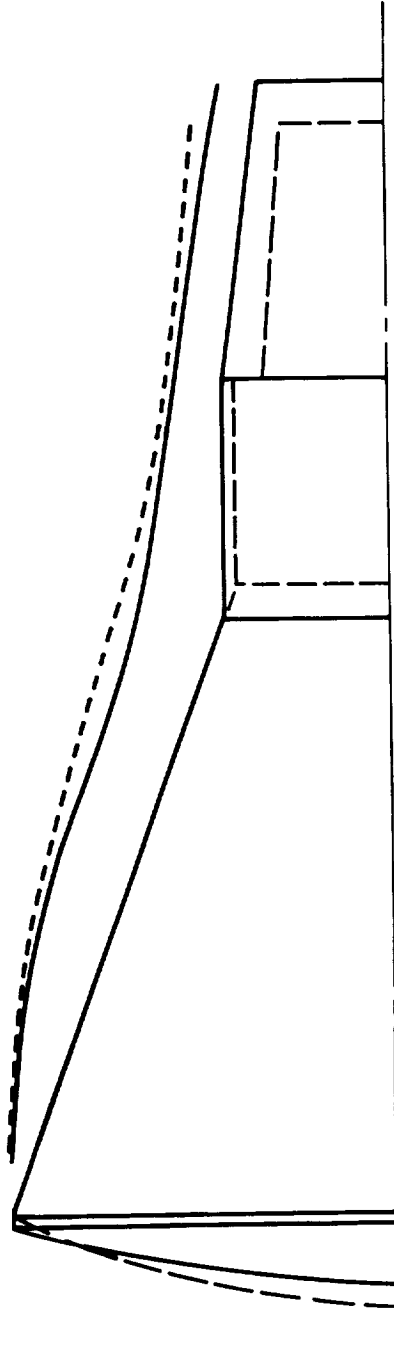
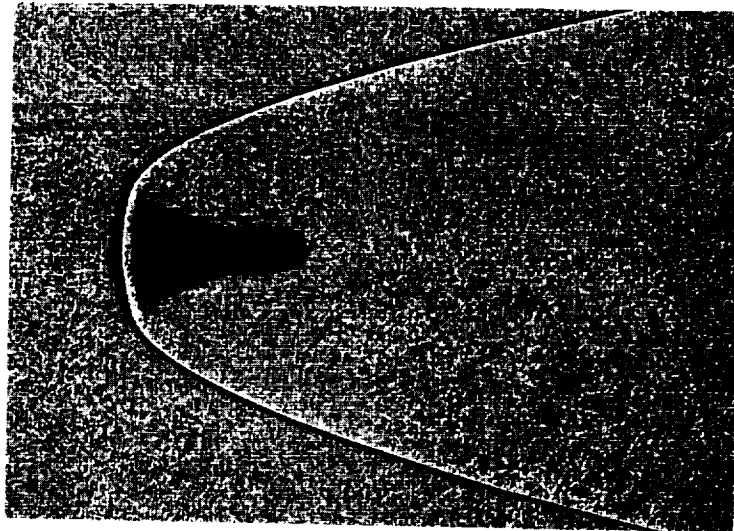
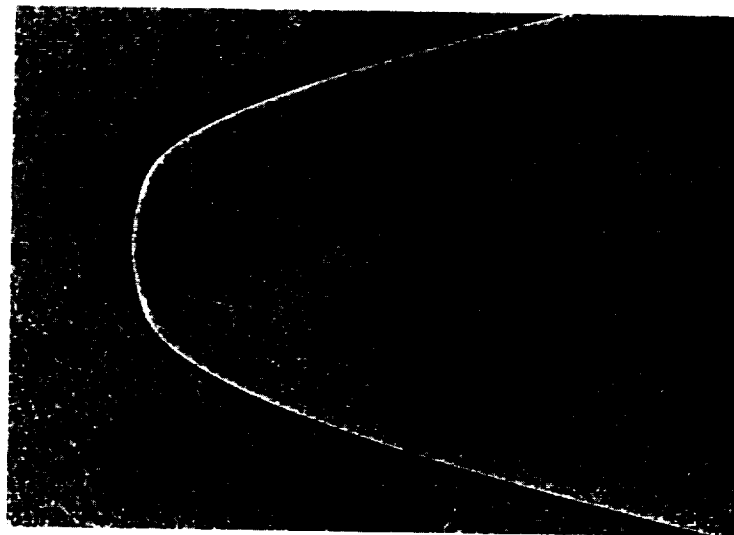


Figure 12.- Comparison of afterbody flow for Gemini and Mercury at Mach number 3.44.



A-31324

(a) Gemini (wind-tunnel test), $\alpha = 2.46^\circ$ ($\beta = -1.02^\circ$), $M = 9.74$, $R = 1.36 \times 10^6$.



A-25025

(b) Mercury (wind-tunnel test), $\alpha = 0.8^\circ$ ($\beta = 1.3^\circ$), $M = 9.75$, $R = 1.47 \times 10^6$.

Figure 13.- Typical shadowgraphs at $M = 9.5$.

~~CONFIDENTIAL~~

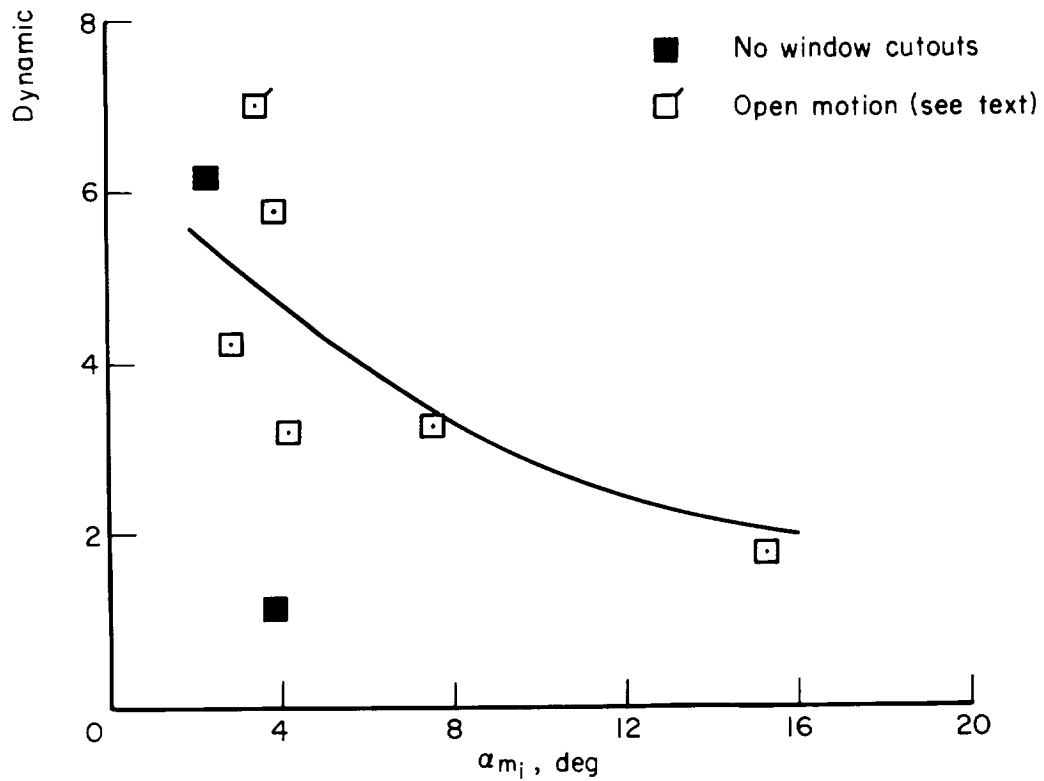
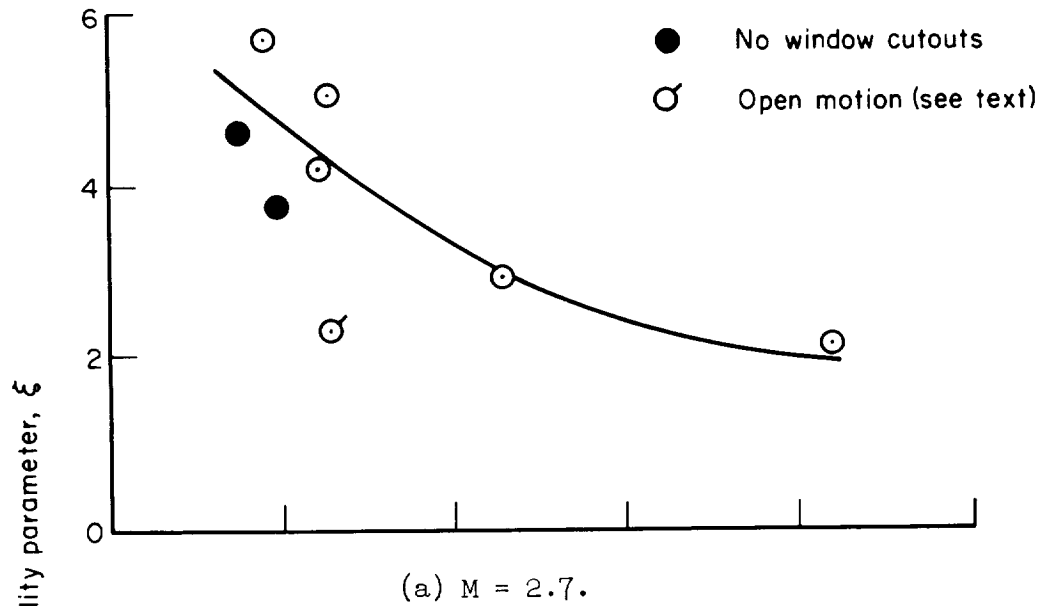


Figure 14.- Dynamic-stability parameter for nominal Mach number of 3.

~~CONFIDENTIAL~~

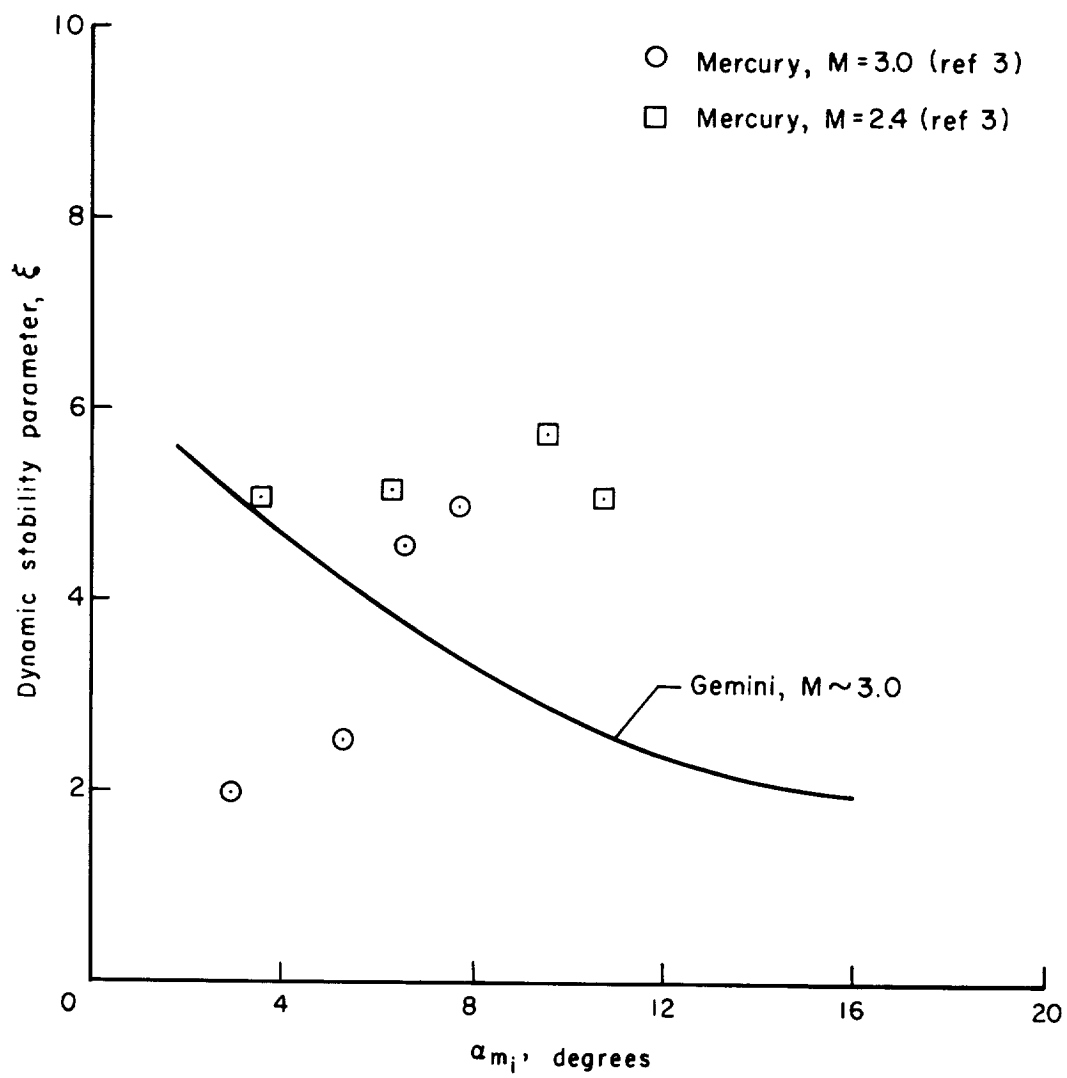


Figure 15.- Comparison of dynamic-stability parameter for Gemini and Mercury at a nominal Mach number of 3.

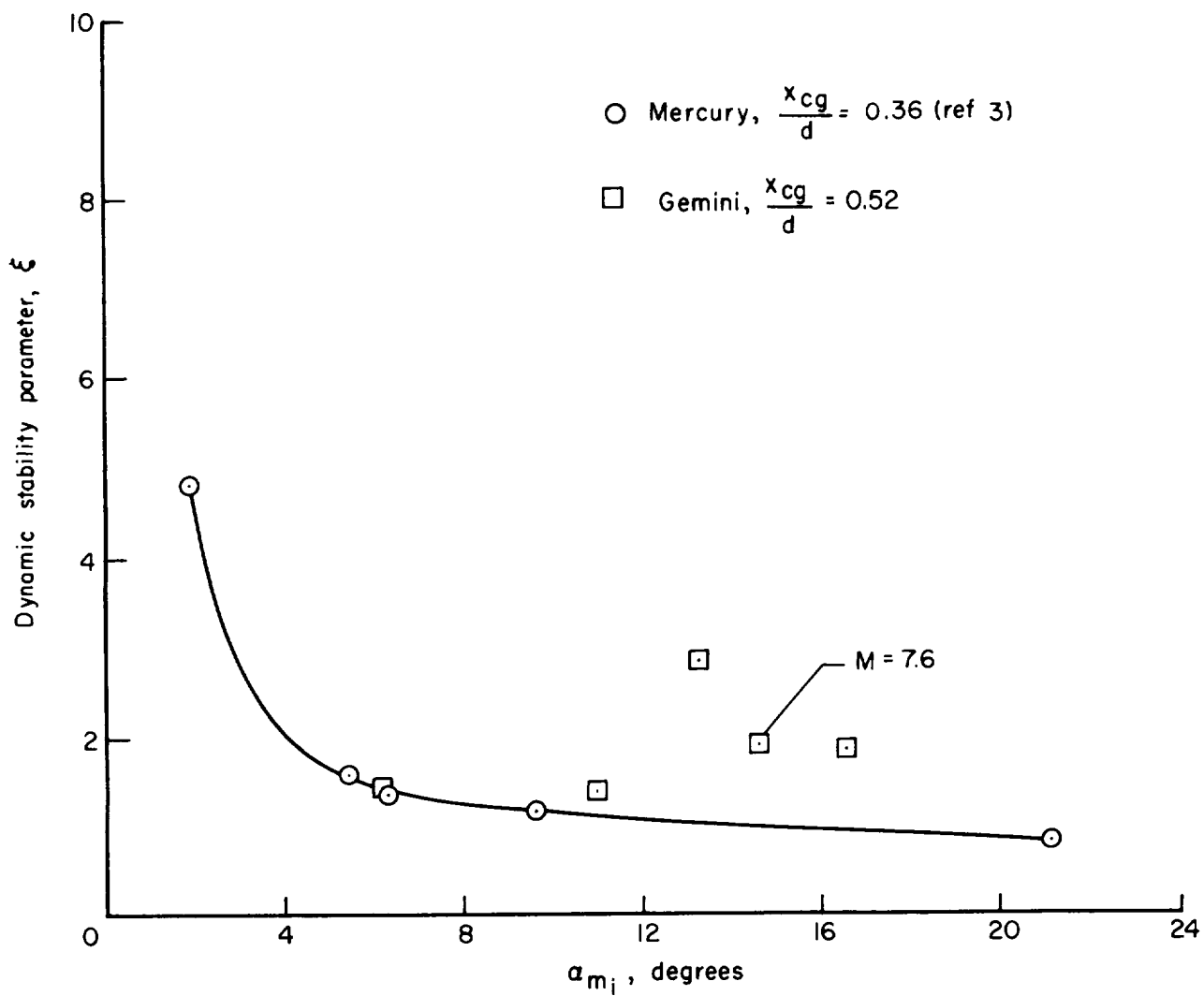
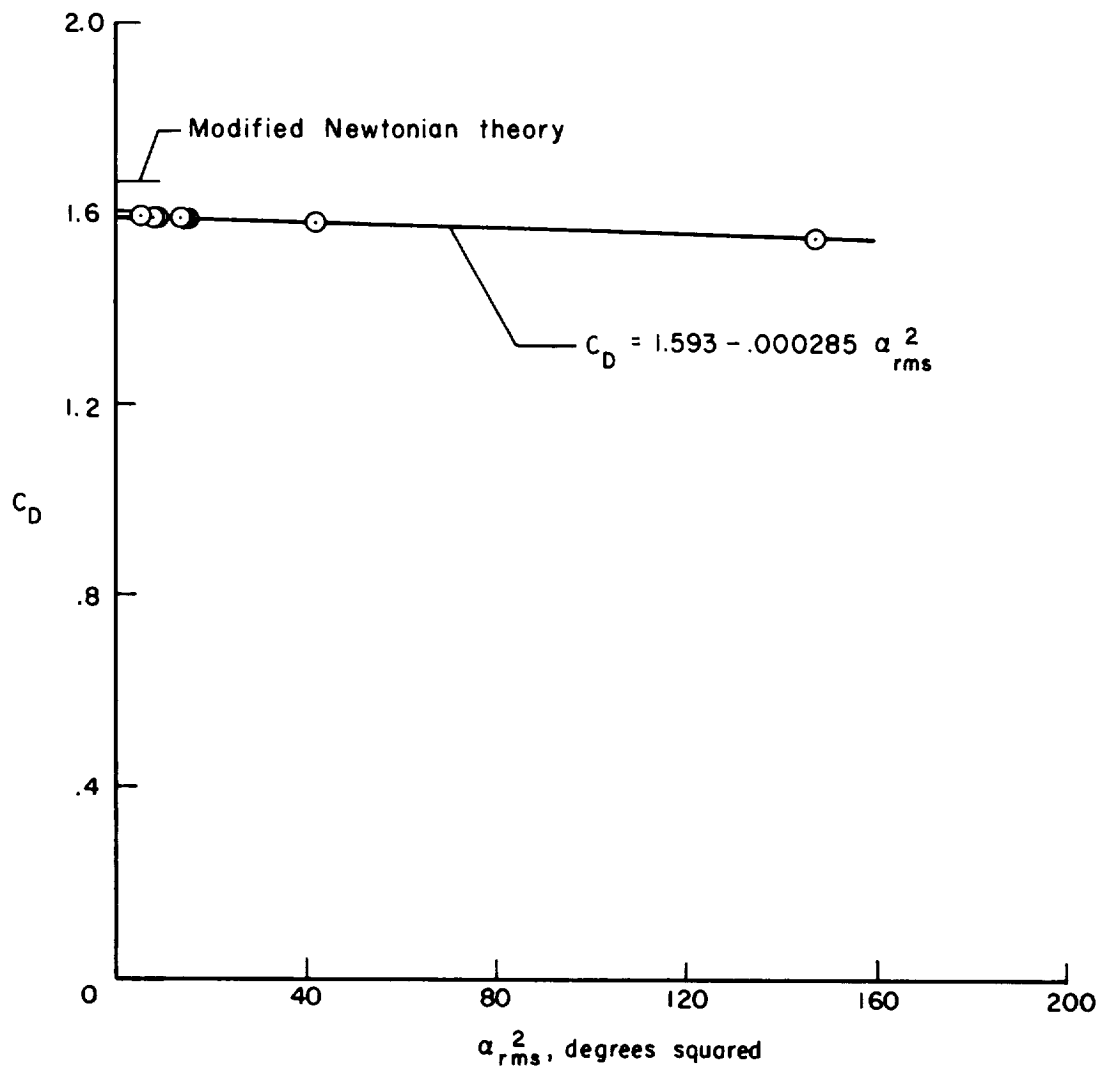


Figure 16.- Comparison of dynamic-stability parameter for Gemini and Mercury at a nominal Mach number of 9.5.

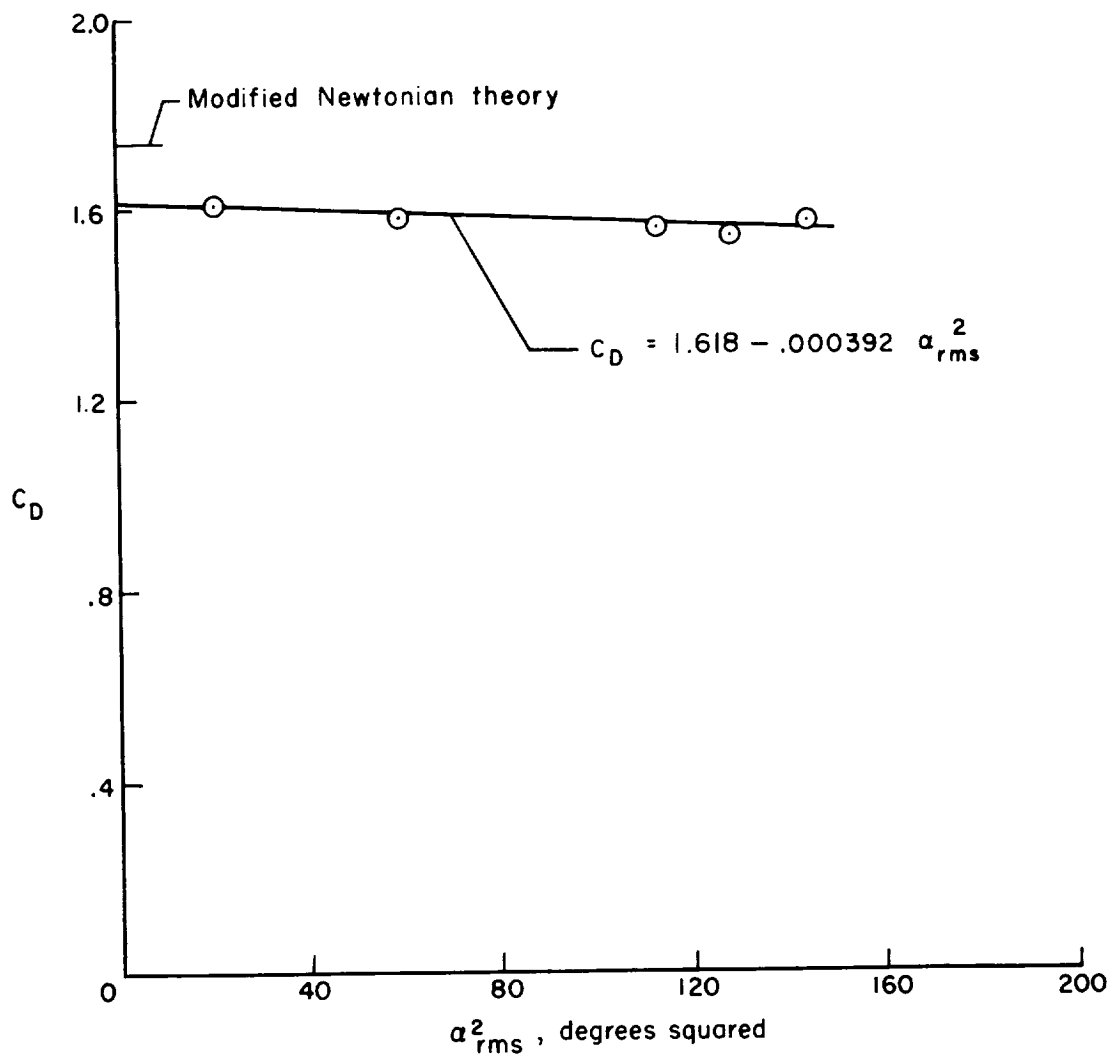
~~CONFIDENTIAL~~



(a) $M \approx 3$.

Figure 17.- Drag coefficient.

~~CONFIDENTIAL~~



(b) $M \approx 9.5$.

Figure 17.- Concluded.

•

•

•

•

|